Transition Metal Ion Interactions with Disordered Amyloid-β Peptides in the Pathogenesis of Alzheimer´s Disease: Insights from Computational Chemistry Studies

Birgit Strodel[1,2] and Orkid Coskuner-Weber[*3]

[1]Institute of Complex Systems: Structural Biochemistry (ICS-6), Forschungszentrum Jülich GmbH, Jülich 52425 Germany, [2]Institute of Theoretical and Computational Chemistry, Heinrich Heine University Düsseldorf, Universitätstrasse 1, Düsseldorf 40225 Germany, [3]Turkish-German University, Molecular Biotechnology, Sahinkaya Caddesi, No. 86, Beykoz, Istanbul 34820 Turkey

Email: b.strodel@fz-juelich.de and weber@tau.edu.tr

KEYWORDS: Alzheimer´s disease, amyloid-β, transition metals, computational chemistry.

"After all, science is essentially international, and it is only through lack of the historical sense that national qualities have been attributed to it". Marie Curie

ABSTRACT: Monomers and oligomers of the amyloid-β peptide aggregate to form the fibrils found in the brains of Alzheimer´s disease patients. These monomers and oligomers are largely disordered and can interact with transition metal ions, affecting the mechanism and kinetics of amyloid-β aggregation. Due to the disordered nature of amyloid-β, its rapid aggregation, as well as solvent and paramagnetic effects, experimental studies face challenges in the characterization of transition metal ions bound to amyloid-β monomers and oligomers. The details of the coordination chemistry between transition metals and amyloid-β obtained from experiments remain debated. Furthermore, the impact of transition metal ion binding on the monomeric or oligomeric amyloid-β structures and dynamics are still poorly understood. Computational chemistry studies can serve as an important complement to experimental studies, and can provide additional knowledge on the binding between amyloid-β and transition metal ions. Many research groups conducted first principles calculations, ab initio molecular dynamics simulations, quantum mechanics/classical mechanics simulations and classical molecular dynamics simulations for studying the interplay between transition metal ions and amyloid-β monomers and oligomers. This review summarizes the current understanding of transition metal interactions with amyloid-β obtained from computational chemistry studies. We also emphasize the current view of the coordination chemistry between transition metal ions and amyloid-β. This information represents an important foundation for future metal ion chelator and drug design studies aiming to combat Alzheimer's disease.

1. INTRODUCTION

Transition metal ions and oxidative metabolism play fundamental roles in Alzheimer´s disease (AD).[1-4] A neurological characteristic of AD is the presence of oxidative stress associated with proteinaceous deposits in specific regions of the brain. Abnormalities in brain transition metal metabolism have also been reported for AD. The pathological pathway underlying AD appears to be linked to increased oxidative damage that results from alterations in neuronal transition metal ion homeostatis. Copper, zinc and iron ions are involved in oxidative mechanisms of neuronal cell death and injury because free transition metal ions promote the generation of reactive oxygen species (ROS).[1-4]

Interestingly, the metal ion metabolism in the brain remains poorly understood while transition metal ion metabolism in several tissues has been studied extensively. Transition metal ions, such as zinc (Zn), copper (Cu) and iron (Fe) exist in the brain. Zn is highly concentrated in the neocortical and hippocampal areas.[5-7] In fact, Zn concentration in the neocortex varies between 150 and 200 μM, which is one order of magnitude greater than that in blood. High cellular concentrations of Cu in the body are not only detected in the liver, but also in the brain.[5-8] There it is most concentrated in the gray matter with concentrations of 60 to 110 μM, which is about one-half order of magnitude greater than the Cu concentration in blood. Similarly, in addition to the liver, the brain contains the highest cellular concentration of Fe in the human body. The greatest nonheme Fe concentrations are detected in the substancia nigra, putamen, caudate nucleus, dentate nucleus, globus pallidus, and intrapeduncular nucleus and high amounts are also found in the hippocampus and cerebral cortex.[5-7,9,10] The Fe concentration in the

brain is about one to two orders of magnitude larger than that in the blood.

The concentration of Zn remains relatively constant in the brain throughout adult life. However, various investigations indicate that the Zn metabolism is altered in AD as significantly elevated Zn concentrations have been found in the hippocampus, amygdala, inferior parietal lobule and olfactory region in AD brained.[5-7] *In vivo* studies demonstrated Cu accumulates in amyloid plaques and participates in the deposition of amyloid-β (Aβ) in amyloid plaques.[8 and references therein] Various investigations also revealed an increased Fe concentration in neocortical gray matter, temporal and frontal pole, inferior parietal, hippocampus, amygdala and the olfactory region in AD brains.[9] The concentration of Zn remains relatively constant in the brain throughout adult life. However, various investigations indicate that the Zn metabolism is altered in AD as significantly elevated Zn concentrations have been found in the hippocampus, amygdala, inferior parietal lobule and olfactory region in AD brained.[5-7] *In vivo* studies demonstrated Cu accumulates in amyloid plaques and participates in the deposition of amyloid-β (Aβ) in amyloid plaques.[8 and references therein] Various investigations also revealed an increased Fe concentration in neocortical gray matter, temporal and frontal pole, inferior parietal, hippocampus, amygdala and the olfactory region in AD brains.[9]

Aβ is a disordered peptide that neither adopts a stable structure in its monomeric nor in its oligomeric form in solution.[11-18] Aβ consists of 36-43 amino acid residues and is involved as the main component of amyloid plaques (Figure 1). Aβ derives from the amyloid precursor protein (APP) following cleavage by the β-secretase and the γ- secretase. Disordered Aβ peptides form highly dynamic oligomers that exist in various forms. Certain misfolded seeds can induce Aβ to also take the misfolded and toxic oligomeric state, which yields a chain reaction akin to prion infection. Misfolded Aβ can also induce tau protein misfolding.[19,20]

Zn, Cu and Fe interact with monomeric and oligomeric Aβ and thereby change the structure and conformational free energy landscapes of Aβ. These interactions are extremely difficult to study using conventional experimental tools due to rapid conformational changes resulting from the disordered nature of monomeric and oligomeric Aβ in solution, the fast aggregation of Aβ, solvent effects as well as paramagnetic effects due to the transition metal. While X-ray crystallography has failed in the determination of the structure of metal-Aβ species, nuclear magnetic resonance (NMR), electron paramagnetic resonance (EPR) and X-ray absorption spectroscopy (XAS) provide limited information.[21-34] Theoretical and computational chemistry studies complement experiments and provide further knowledge on the interactions of transition metals with monomeric and oligomeric Aβ in solution at the electronic, atomic and molecular levels. Extensive density functional theory (DFT) calculations, ab initio molecular dynamics (MD) simulations, quantum mechanics/molecular mechanics (QM/MM) simulations, and classical MD simulations–with and without enhanced sampling–have been conducted to study transition metal ion bound Aβ peptide monomers or oligomers in solution. In this study we provide a review on the contribution of theoretical and computational chemistry to characterize the structural and thermodynamic properties of transition metal ion bound Aβ. We also offer a future perspective in this field and the major challenges that are required to be solved to design chemical and biological treatments for AD targeting the influence of transition metal ions during disease development.

2. Metal Ions and Aβ: Insights from Experiments

2.1 Zn and Aβ

Various coordination sites have been proposed for the binding of Zn(II) to Aβ (see Table 1). Because of the d^{10} electronic configuration, Zn(II) measurements using conventional spectroscopic techniques, such as EPR and UV-vis, are challenging.[35] Therefore, the coordination mechanism can be characterized using X-ray absorption spectroscopy (XANES or EXAFS). XANES provides valuable structural information, but requires the simulation of the spectra in order for more quantitative data to be obtained. The development of simulation approaches is an active research area in various groups, but requires an initial structural dataset that is provided by experiments, such as X-ray crystallography.[36] Such structural data are not available for Aβ bound to Zn(II) and therefore XANES measurements of these complexes can yield inaccurate results.[35] EXAFS measurements, on the other hand, can provide information about the number, nature and ligand distances binding to Zn(II) but in this case (regarding disordered Aβ peptides) the recorded studies suffer from not well-defined Zn(II) coordination sphere and useful oscillation number is limited.[35] Therefore, we can only define the Zn(II) ion´s first coordination sphere with Aβ. EXAFS measurements show that the oscillations are more accurately produced with a 4NO coordination shell with an average distance of 1.98 Å from Zn(II).[35] The bond-valence-sum theory results yield an oxidation state of 2.08 for Zn when it is four-coordinated but it yields an unrealistic value of 2.60 when it is five-coordinated.[35] These findings strongly supported a tetrahedral coordination mode for Zn(II), which is also the most common coordination geometry for Zn(II) in biology.

Another experimental technique for studying the coordination ligands of Zn(II) is to measure how its coordination effects the NMR spectra of binding ligands of Aβ.[35] The effect may be broadening of some protons or their down- or upfield shift.[35] These approximations can provide information about the binding of Zn(II) in the close vicinity of protons leading to Lewis acidity changes or indicate Aβ conformational changes caused by Zn(II) coordination.[35] Zn(II) first coordination sphere modes from NMR measurements are not fully concurrent. Discrepancies might be because of different experimental conditions (length of the peptide, buffer, pH and temperature etc.) and means utilized for increasing Aβ solubility (PEGylated counterparts, N-terminal acetylation of Aβ, water-micelle environment etc.).[35] For example, most recently, Alies et al. used NMR measurements for elucidating the Zn(II) coordination

sphere.[35] Protons of the three His residues were found to be affected by Zn(II) binding with the three His Hδ being slightly down-shifted and one of them showed broadening.[35] Both protons from Tyr10 were also down-shifted and Hδ possessed a stronger shift. The most pronounced changes for the Hα atoms induced by the metal were (i) a strong broadening for Val12, (ii) a down-shift for Asp1 and Glu3, and (iii) an up-shiftwith a quite intense broadening for Glu11.[35] For the Hβ region, the two diastereotopic Asp1 Hβ1 and Hβ2 were brought closer, the Ala2 Hβ was weakly down-shifted, and the Asp7 Hβ up-shifted.[35] Lastly, a broadening of Val12 Hγ1 was clearly observed as well as a slight broadening and down-shift of the Arg5 Hγ.[35] From this data, it was challenging to determine the Zn(II) coordination sphere. NMR study alone was not capturing all details because more than four binding groups are affected by the presence of Zn(II). These findings are in line with what has been observed for several possible sites in equilibrium for Cu and Fe with Aβ.[35]

To gain more insights, Alies et al. conducted recently XANES and NMR measurements of Zn(II) binding to several modified species.[35] We should mention here that mutations affect the biochemical and biophysical characteristics of Aβ.[37] XANES measurements supported a four-coordinated metal center. Thus (i) supporting the conclusions from the EXAFS data for the same Zn:Aβ species and (ii) revealing that a mutated residue that is no longer able to bind to the Zn(II) ion is replaced by another residue ligand, keeping the coordination number at four in the Zn(II):Aβ complexes.[35] Apart from Zn:E11Q-Aβ, all other complexes yielded spectral signatures of biological systems with two His residues bound (and a coordination number of four).[35] The spectrum of the E11Q mutant rather resembled that of a system with three His ligated to Zn(II), indicating that the missing Glu11 is replaced by the third His residue in this complex.[35] For identifying His with the strongly broadened Hδ signal (see above), the three His-to-Ala mutants were studied.[35] It was found that while all three His residues can bind to Zn(II), they do so to different extents. Specifically, the strong involvement of His13 and His6 was concluded from the disappearance of the broadening of the Val12 and Arg5 resonances in the Zn(II):H13A-Aβ and Zn(II):H6A-Aβ complexes.[35]

The interactions between Zn(II) and the carboxylate groups were elucidated by comparingthe impact of Zn(II) on the Aβ peptide and its mutants.[35] Following results were obtained: (i) with an amidated carboxylate group of D1; (ii) Zn(II) had similar effects on Aβ and the E11Q-mutant, indicating that Glu11 does not interfer with the binding of Asp1 to Zn(II); (iii) with mutants, E3Q-Aβ and D7N-Aβ, an intermediate state was observed. Zn(II) affects the Asp1 and Ala2 Hβ but differently than the data for Aβ.[35] These studies suggested that Zn(II) coordinates to Glu3 and Asp7.[35] It was proposed that Asp1, Glu3, and Asp7 are reactive towards for Zn(II), while Glu11 binds to Zn(II) independent of the other carboxylate residues.[35]

pH dependence of modifications on the Asp1 Hα and Asp1 Hβ of the Aβ and Ac-Aβ peptides upon Zn(II) binding were investigated.[35] For the Asp1 Hα, there was a down-shift and a weak broadening at pH 7.4 even though the broadening was more starker at pH 9.0, with an up-shift in the presence of Zn(II).[35] Side chain of Asp1 rather than the N-terminal amine coordination to Zn(II) was detected as a modification by Zn(II) coordination.[35] The situation was different at a pH of 9.0 because the detected broadening was no longer observed for the Ac-Aβ.[35] Additionally, Zn(II) coordination affected also the N-terminal region (Ala2 Hβ).[35] Ala2 Hβ of the Aβ peptide broadening occurred when the pH was increased from 7.4 to 9.0. However, this effect was not observed for the acetylated Aβ.[35] Zn(II) coordination to the N-terminal amine induced a broadening of the Ala2 Hβ, which was observed at a pH of 9.0.[35] Asp1 Hβ2 and of the Ala2 Hβ of the Aβ peptide at pH 9 compared to pH 7.4 demonstrated a stronger broadening with Zn(II) coordination. That was an effect not observed with the Ac-Aβ, suggesting that the N-terminal amine is not coordinated to Zn(II) at a pH of 7.4.[35]

2.2 Cu and Aβ

Cu ions are associated with Aβ aggregation and ROS production processes, which are two modifications encountered in AD pathology. Cu coordination region (residues 1-16) is located next to the CHC region (residues 17-21) and the redox properties of Cu are linked to the Cu ion coordination environment.[39] In the last two decades, many investigations were conducted on this subject, yielding debated results (Table 2). These were discussed in Ref. 38 in detail. Here, our aim is to provide a plausible illustration for Cu(II) binding to Aβ using computational chemistry that was initiated from the many various experimental investigations. Discrepancies between experiements may result due to the disordered nature of Aβ structure.

As mentioned above, the Cu(II) ion coordination site of Aβ is located in the N-terminal region. Therefore, the Aβ(1-16) fragment has been very often used in experimental and computational studies.[39 and references therein] However, we should note that the chosen fragment size effects the biochemical and biophysical properties of disordered Aβ.[40] A second Cu(II) binding site has been shown as well when the peptide is considered as a 1-28 fragment or longer.[39 and references therein] Sequent two sites were demonstrated for Cu binding. Several studies demonstrated only one coordination site, however, this may be due to the lower affinity of Cu(II) for the second site, precluding its detection.[39 and references therein] The buffer used in experiments influences the outcome as well. For instance, it is more challenging to detect the second binding site in a buffer with a strong affinity for Cu(II), such as TRIS.[39] Interestingly, an additional study demonstrated that two Cu(II) ions coordinate with Aβ(1-28) but only one Cu(II) ion binds to Aβ(1-42) in aqueous solution.[39 and references therein] In the presence of methanol, the second Cu(II) site in Aβ(1-42) is accessible. Steric

hindrance of the 2nd coordination site affected by the hydrophobic tail of Aβ(1-42) that might be associated with these findings in comparison to Aβ(1-28). Such interactions are very sensitive to additives in the experiments, such as alcohols.[39] However, not much is known about the second Cu(II) coordination chemistry. The Cu(II) coordination may be 2N2O or 3N1O based on EPR measurements and Cu(II) coordination to the second site seems not to interfere with Cu(II) binding to the high-affinity site of Aβ.[39 and references therein] Regarding the binding affinity, the first high affinity binding site of Aβ is at least two order of magnitude stronger than the second binding site. When we consider that Cu ions were observed in Aβ plaques, the second binding site might not be existing *in vivo*. Formation of $Cu_2(A\beta)_2$ complexes was also reported but this was ruled out later.[39]

An anamnesis feature between the different studies on Cu(II) coordination to Aβ is the coexistence of two compounds depending on pH, usually marked as species I that is predominant at lower pH and II that exists at higher pH.[41] These two species possess dissimilar spectroscopic features in CD, EPR, XAS, NMR and UV-vis measurements.[39] The transition pH value between species I and II is close to pH 7.8 with small deviations between investigations due to divergent sample preparation protocols. It has also been reported by potentiometry and calorimetry experiments that species II is obtained from species I by Aβ deprotonation. More details can be found in Ref 39.

Predominant species at lower pH is formed by two equivalent sets of equatorial ligands where the Asp1 N-terminal $-NH_2$, theAsp1-Ala2 CO bond, a His6, His13 and His14 N atom are comprised in the coordination sphere.[39] The two components are in 1:1 ratio and in equilibrium. These are noted as species I. Regarding species II that is predominant at higher pH, there have been two hypotheses: it was proposed that species II is made of the CO group from the Ala2-Glu3 peptide bond and the imidazole rings of the three His residues based on HYSCORE and S-band EPR data on ^{13}C and ^{15}N isotropically labeled peptides.[39] Regarding the apical coordination, the debate continues, however, carboxylate group involvement was demonstrated.

The Cu(II) coordination mechanism in Aβ fibrils or aggregates is investigated utilizing EPR measurements. These studies showed that an unchanged Cu(II) coordination shell between soluble monomeric and insoluble oligomeric Aβ species.[39] The second Cu(II) binding site that is detected in Aβ(1-28) fragment may not be retained in fibrils due to reasons explained above. Cu(II) affinity for soluble monomeric and fibrillary forms are akin, indicating similar Cu(II) binding characteristics in both forms. However, we should mention here that similar spectroscopic signatures and affinity do not indicate identical Cu(II) binding modes. Solid state NMR studies proposed the involvement of Glu side chains, C-terminus carboxylate group and of N^{τ} atom of His13 and His14. NMR measurements of soluble Aβ peptides show that all carboxylate groups were impacted by Cu(II) paramagnetism.[39] The His13 and His14 N atom (imidazole ring) is coordinated to Cu(II) differs from that was demonstrated for the soluble Aβ peptide (N^{π}). This is still a modification that cannot be explained in mechanism and might be caused due to a rearrangement in His residues in fibrils in comparison to soluble Aβ.

Cu(I) is coordinated through two His residues in a linear mode as proposed by experiments comparing truncated Aβ(6-14) and Aβ(10-14) fragments and synthesized His13-His14 dyad models as well as XAS measurements.[39] From Aβ fragment studies, His13-His14 dyad were proposed as the one responsible coordination site for Cu(I) binding. This was supported by ESI-MS measurements. However, ^1H-NMR measurements proposed that Cu(II) binds to three His residues. O_2 activation was demonstrated to depend on His binding.[39] Therefore, it might be crucial in ROS production mechanism. XAS measurements showed that Cu(I) binds to Aβ in a tetrahedral fashion. An increased reactivity toward O_2 for the oligomeric rather than monomeric form was detected and this behavior was linked to differences in coordination geometry, *i.e.*, tetrahedral vs. linear. Affinity measurements were conducted using various methods including alanine scanning and these studies showed that only two His residues are required for Cu(I) coordination. The His6Ala mutant peptide was the one with stronger Cu(I) affinity in comparison to the His13Ala and His14Ala mutant peptides.[39] However, our recent studies clearly show that alanine scanning method impacts the predicted biochemical and biophysical properties of Aβ (see above).[37]

2.2. Fe and Aβ

Because of the stable Fe(III) hydroxide species precipitation, Fe(III) to Aβ coordination is impossible.[39] A ternary complex formation including the NTA ligand was reported.[39] The interaction of Fe(III)-porphyrin with Aβ was detected as well, where Aβ is coordinated to hemic Fe(III) through Arg5 via a hydrogen bond network with a water molecule and through the His13 imidazole group.[39] As Fe(II) is air-sensitive and is being oxidized to Fe(III) upon exposure to air during experimental measurements, The formation of Fe(III) hydroxo species inhibits the detection of Fe(II)-Aβ interactions.[39] Detection of Fe(II) coordination with Aβ under physiological conditions was achieved by ^1H, ^{13}C and 2D NMR measurements. Asp1, Glu3, and the three His residues are involved in Fe(II) binding based on these experiments.[39]

2. Computational Chemistry Studies of Transition Metal-Aβ Complexes

2.1 Density Functional Theory Calculations

DFT is a method used in biology, chemistry and physics for investigating the electronic structure of many-body systems like atoms and molecules. Using DFT, many-electron system properties can be calculated by using functionals, which depends on

spatially dependent electron density. Usually, hybrid DFT computations have been utilized in the studies of metal and Aβ interactions. These are a set of approximations to the exchange-correlation energy functional, which capture a part of Hartree-Fock theory´s exact exchange with the rest of the approximations belonging to studies to exchange-correlation energy from empirical or ab initio sources. Kohn-Sham orbitals are used for the exact exchange energy functional expression. The linear combination of the Hartree-Fock exact exchange depends on a hybrid exchange-correlation functional that is generally computed as a Hartree-Fock exact exchange functional linear combination, E_x^{HF}:[42]

$$E_x^{HF} = -\frac{1}{2}\sum_{i,j}\iint \psi_i^*(r_1)\psi_j^*(r_2)\frac{1}{r_{12}}\psi_j(r_1)\psi_i(r_2)dr_1dr_2$$

One of the most commonly utilized versions is Becke, 3-parameter, Lee-Yang-Parr (B3LYP) level of theory and its exchange-correlation functional is:

$$E_{xc}^{B3LYP} = E_x^{LDA} + a_0(E_x^{HF} - E_x^{LDA}) + a_x(E_x^{GGA} - E_x^{LDA}) + E_c^{LDA} + a_c(E_c^{GGA} - E_c^{LDA})$$

where $a_0 = 0.20, a_x = 0.72$ and $a_c = 0.81$ $are\cdot$ E_x^{GGA} and E_C^{GGA} are generalized gradient approximations; the Becke 88 exchange functional and the Lee, Yang and Parr correlational functional for B3LYP and $E_C^{LDA}$is the VWN local-density approximation to the correlation functional. B3LYP is defined by three parameters and these were adopted from Becke´s initial fitting of B3PW91 functional to a class of atomic energies, proton affinities, ionization potentials and total atomic energies. Such calculations have been widely conducted for elucidating transition metal-Aβ coordination chemistry details. We summarize the major results for Zn, Cu, Fe and Pt interacting with Aβ that were obtained using DFT calculations.

Cu and Zn Interactions with Aβ:

H_2O_2 production is implicated in Aβ neurotoxicity and Cu-Aβ complexes in the vicinity of a reducing substrate, such as dopamine or ascorbate, catalyze the production of H_2O_2 in order to identify the molecular mechanism of this reactions, Bush and co-workers performed DFT calculations and presented a mechanism with a pivotal role for Tyr10, which was supported by mutagenesis experiments.[43] They used the B3LYP density functional along with the LANL2DZ basis set for modeling the reaction mechanism utilizing small truncated models. The ground state, transition state, and product structures of the model phenol-OOH system were optimized using the B3LYP functional along with the 6-31G** basis set. Stationary points were checked by means of frequency calculations and unscaled frequencies were used to obtain zero-point energies. Solvation effects were included using a continuum model for water. LACVP basis set was utilized in these studies. Based on their findings, the catalytic reduction of O_2 to H_2O_2 requires Cu-Aβ acting as a two-electron redox unit by having two distinct one-electron acceptors, Cu(II) and an Aβ free radical localized on Tyr10. They showed that the catalytic activity of Cu-Aβ resembles that of galactose oxidase, which is a cupro enzyme that has His and Tyr residues in its coordination sphere and oxidizes primary alcohols to aldehydes while O_2 is reduced to H_2O_2. The Cu ion has initially a +2 oxidation state in their calculations, which is reduced to +1 via a hydrogen atom transfer from the substrate to a coordinated Tyr residue. This mechanism causes Tyr to dissociate from copper, leaving Cu(I) in a trigonal coordination fashion that is subsequently able to coordinate and reduce O_2. Along with their experimental measurements, Bush and co-workers suggested that dityrosine cross-linked oligomers were the toxic species. They further proposed a mechanism for the formation of such Tyr cross-linkages via oxidative modification. Overall, they provided a chemical mechanism from B3LYP calculations using truncated Cu-Aβ models for how Cu-Aβ interactions catalytically generate H_2O_2. They stated that Tyr10 redox activity is a novel biochemical target that may possess therapeutic promise for AD. About a decade later, Coskuner and Uversky demonstrated that the presence of Tyr10 in the primary structure of Aβ regulates the formation of toxic β-sheets in the structural ensembles of the Aβ42 monomer in aqueous solution obtained from replica exchange molecular dynamics (REMD) simulations, yet without the presence of metals.[44] The role of Tyr10 in the structures of Aβ in the presence of transition metal ions still remains to be elucidated.

In a cell environment with an oxidative stress cascade initiated in mitochondria region, where high levels of H_2O_2 exist along with a reducing environment (gluthathione or ascorbate), Cu(I)-Aβ is expected to enhance the radical cascade by reducing hydrogen peroxide and generating toxic hydroxyl radicals. Prosdocimi *et al.* evaluated the reactivity of different Cu(I)-Aβ coordination modes proposed in the literature in terms of OH radical production using DFT calculations.[45] To this end, they used the BP86 functional along with the def2-TZVP basis set and a continuum water model for modeling solvent effects. For each coordination mode considered in their study, they modelled the corresponding H_2O_2 adduct and conducted potential energy surface scans along the reaction coordinate of O-O bond dissociation of the peroxide resulting in the production of two OH radicals, and obtained thermodynamic reaction profiles. They found that the experimentally postulated Cu(I)-Aβ coordination geometry with two His residues in the coordination sphere is not capable of performing efficient H_2O_2 reduction. On the other hand, they also experimentally proposed Cu(I)-Aβ complex with three His residues coordinating to Cu(I) is capable to produce OH radicals. Recent studies including the one proposed by Prosdocimo *et al.* (see above) indicated the involvement of three histidine residues (His6, His13 and His14) in the coordination chemistry between Aβ and metal ions. The fourth ligand is assumed to be most likely an oxygen atom coming either from Tyr10, the Asp1 carboxylate group or other carboxylate side chains. But also the N-terminal nitrogen has been proposed as fourth ligand. Zirah *et al.* and Gaggeli *et al.* suggested that Glu11 provides the carboxylate side chain in Zn-Aβ16 and Zn-Aβ28, while the Asp1 side chain forms a hydrogen bond to an axial water located in the first coordination shell of Cu(II).[46-48] From x-ray absorption fine structure measurements of Cu(II)-Aβ16 and Cu(II)-Aβ40 penta-coordinated Cu(II) bound to three nitrogen atoms (His6, His13 and His14)

and two oxygen atoms was proposed. These oxygen atoms belong to Tyr10 and a water molecule or an amino acid residue different than the already coordinated His and Tyr residues. However, other studies concluded that Tyr10 is not the oxygen donor. Aspartate and glutamate have been detected very often in the coordination spheres of Zn and Cu while tyrosine coordination has been rarely observed. The different findings for the binding modes between transition metal ions and Aβ have been explained by the differences in peptide preparation, pH, buffer conditions, and concentration.

First principles calculations have been conducted extensively to resolve this debate. For instance, Streltsov *et al.* used DFT computations with the B3LYP functional and the LANL2DZ basis set for optimizing the structures of Cu(II) bound Aβ via modeling the system by a Cu(II) ion coordinated to Asp, Glu or Tyr and the imidazole rings.[49] For the geometry optimizations, the modified geometry optimization by direct inversion in the iterative subspace (GDIIS) algorithm and tight convergence criteria were utilized. The true energy minima were computed using stationary points for frequency calculations. They found a Jahn-Teller type distorted octahedral coordination about Cu(II) and reported the bond lengths and bond angles for these geometries. The optimized structures were then utilized in the extended X-ray absorption fine structure (EXAFS) spectra data refinements, based on which a distorted hexa-coordinated structure around Cu(II) with three His, a Glu and/or Asp residue and an axial water molecule as ligands was reported.[41] It was further concluded that this coordination geometry yields a better fit of the EXAFS data than the octahedral Cu(II):Glu/3His/water geometry. They found three His nitrogen atoms and one of the Glu carboxylate oxygen atoms to coordinate Cu(II) in a distorted square planar equatorial arrangement while the other carboxylate oxygen atom and the oxygen atom of the water molecule are in an axial a position. These studies were followed by Marino *et al.*,[50] who performed DFT calculations using the B3LYP functional and the 6-31G(d) basis set for C, O, N and H atoms, the Stuttgart energy-averaged effective core pseudopotentials (ECP) for the core electrons of Zn and Cu, and a consistent basis set introduced by Dolg *et al.* for the valence electrons of the metal ions. They investigated the possible coordination of three His residues along with Asp1, Tyr10 or Glu11 to Zn(II) and Cu(II) ions. The chosen models involved 4-methylimidazole for His, phenol for Tyr, and acetate for Glu or Asp. Their calculations revealed that Zn(II) forms four- to five-coordinated species while Cu(II) has a preference for five-coordinated geometries. Probable oxygen donor ligands were reported to be Asp or Glu, and water exhibited a higher affinity than Tyr for binding to the metal ions.[50]

Recently, Coskuner-Weber presented the structures and thermodynamic properties of Cu(II):His_3Asp, Cu(II):His_3Tyr, Cu(II):His_3Glu and Cu(II):$His_3(H_2O)$ as possible coordination configurations using the B3LYP functional along with the 6-31G*, 6-31G**, cc-pVDZ, ahlrichs-vdz, ahlrichs-vtz, def2-svpd, def2-tzvp and lanl2dz-ecp basis sets to understand the impacts of the chosen basis sets on the predicted structures and thermodynamic properties in an extensive set of calculations (Figure 2). The resulting order of binding energies from the largest negative to the smallest negative value is Asp > Glu > Tyr > H_2O based, which agrees with experimental findings by Mantri *et al*. who observed the same trend for Asp, Glu and Tyr.[51]

Mirats *et al.* conducted DFT calculations for several Aβ-Cu-O_2 models using the M06-2X exchange correlation functional along with the 6-31+G(d) basis set for C, N, O ahd H atoms and the LANL2DZ basis set for Cu.[52] Solvent effects were treated utilizing an implicit model for water. The peptide was represented by DGGGGHD-$NHCH_3$ and CH_3CO-HH-$NHCH_3$, which in turn represented the Aβ(1-7) and Aβ(13-14) sequences. Charge transfer to superoxide is associated with spin densities. Formation of superoxide is more favorable in His involved distorted Cu coordination fashions or with the coordination of a ligand, such as Asp1. They did not investigate the superoxide dismutase activity of the Cu: Aβ species because the approach of O_2^- to Cu(II): Aβ was not studied. This still remains to be studied.

Sodupe and co-workers conducted DFT calculations along with homology modeling. The initial geometry was taken from Zn(II):Aβ (PDBID: 1ZE9). The Zn(II) ion was replaced by Cu(II). Overstabilization of Cu(II):ligand structures with lower coordination were reported in QM calculations using GGA or hybrid functionals. Hybrid B3LYP or BLYP functionals yield a four-coordinate structure rather than five-coordinated structure. MPWB1K and BHLYP functionals that have higher percentage of exact exchange are in accord with CCSD(T) results and yield quasi-degenerate structures. For these reasons, Sodupe and co-workers conducted the calculations using a meta-hybrid M06-2X functional. The LANL2DZ pseudopotential was used for Cu and the 6-31G(d) basis set was used for the rest of the atoms. Single point calculations on optimized structures were conducted using single-point energy calculations with the larger LANL2TZ basis set for Cu supplemented with a f function and the 6-311++G(d,p) basis set for the nonmetallic atoms. Solvent effects were considered using a continuum model for water. The rigid rotor approximation along with unscaled harmonic vibration frequency analysis were conducted for estimating thermodynamic corrections. They used the Aβ(1-16) fragment in these calculations. They also used different coordination modes shown experimentally at different pH values. With these modes, they calculated the standard reduction potential and computed the structures and their redox behavior. Their data showed that Cu reduction yields $CO_{backbone}$ decoordination that for distorted square planar structures in the oxidized state leads to tri-coordinated species. For the initially penta-coordinated species with Glu11 at the apical position, leading to a distorted tetrahedral structure. More details can be found in Ref. 53.

Fe Interactions with Aβ:

As for Cu and Zn is the coordination of Fe to Aβ controversely discussed due to contradicting experimental results. Miura *et al.* studied Fe(III)-Aβ complexes using Raman spectroscopy and proposed that Fe coordinates to Aβ through the Tyr10 phenolic oxygen atom, the His residues do not bind like to Fe(III).[54] Despite, Nakamura *et al.* suggested that His6, His13 and His14

are associated with the redox activity of Fe in the senile plaques following experimental studies on the redox behavior of Cu(II) and Fe(III) in the vicinity of Aβ.[55] To resolve this debate, Sodupe, Rauk and co-workers performed structural optimization of truncated models of the Fe(III)-Aβ complex using DFT calculations with the B3LYP functional and the 6-31+G(d) basis set.[56] For obtaining more accurate energies, they increased the basis set size to 6-311+G(2df,2p) and conducted single point energy calculations on structures that were optimized with the smaller basis set. Additionally, they conducted MP2 calculations for evaluating the relative energies and used a continuum model for water for computing the free energy of solvation for different coordination modes. Their results showed that the most preferred complexes containing His13 and His14 and the phenolate group of Tyr10 are the penta-coordinated $[Fe(II)(O\text{-}HisHis)(PhO^{-})(H_2O)]^{+}$ and $[Fe(III)(N\text{-}HisHis)(PhO^{-})(H_2O)]^{+}$ models. In addition, they concluded that coordination of Tyr10, His13 and His14 to Fe(II)/(III) is thermodynamically stable in solution at physiological pH. Their DFT calculations supported the experimental results presented by Miura *et al.*

Pt Interactions with Aβ:

While most studies focused on transition metals with biological importance, *i.e.* Zn, Cu and Fe, recent studies also investigated the interaction of Aβ with organometallic compounds involving metals that are not of pathological importance but represent prototypes for potential therapeutics. Barnham *et al.* illustrated that Pt(II):phenanthroline species repress Aβ aggregation *in vitro*.[57] In general, Pt(II) complexes are kinetically stable and redox inert, indicating that a coordinated Pt(II) would be difficult to be replaced by other metal ions. Thus, Pt complexes could take over the Zn, Cu or Fe binding sites of Aβ and prevent toxic Aβ oligomerization and aggregation. Streltsov *et al.* performed mass spectrometry (MS), XAS and dynamic light scattering (DLS) experiments along with DFT calculations to propose structural geometries for Pt and Aβ interactions.[58] For complex formation between Aβ16 and cis-diamminedichloridoplatinum(II) (cisPt), the best match between theory and experiment was obtained for a mixture of the models where the Cl and NH_3 ligands in cisPt were gradually replaced by histidines and possibly the N-terminus (Asp1), C-terminus (Lys16), and Asp7: Pt–(NH3)2Cl2, Aβ16(His)–Pt–(NH3)2Cl, Aβ16(His)2–Pt–(NH3)2 and Aβ16(His)3(N/O)–Pt. In the case of the cisPt–Aβ42 complex, the best fit was obtained with a mixture of two species: Aβ42(His)3S(Met35)–Pt and Aβ42(His)2S(Met35)–Pt–(NH3).

One should note that the above mentioned and further DFT studies were conducted in the gas phase or using a continuum (but not explicit) model for water, and often used a truncated, small-size model for metal-Aβ complexes instead of modeling the full-length Aβ peptide. Moreover, the dynamics of the disordered Aβ peptide and its interactions with metal ions were also not simulated in these studies as such large size metallopeptides still represent a significant challenge for current first principles methods, such as DFT.

2.2. First Principles Molecular Dynamics Simulations

A simplified version of the many-electron Schrödinger equation can be provided when electrons are divided in two classes: inner core and valence electrons. Inner shell electrons are firmly bound to the nucleus and thus are assumed to not to play a critical role in the chemical binding of atoms; these electrons screen the nucleus partially, therefore, forming a virtually inert core with the nucleus. Transition metal ion binding properties depend on valence electrons. Separation of electrons proposes that inner core electrons can be ignored; reducing the perspective of an atom to an ionic core that interacts with the valence electrons. The utilization of a pseudopotential, effective interaction, approximates the potential felt by the valence electrons. This approximation was first proposed by Fermi in 1934 and Hellmann in 1935.[59,60] The Car-Parrinello molecular dynamics (CPMD) method, which was introduced by Roberto Car and Michele Parrinello in 1985, makes use of this perspective.[62] CPMD is associated with the more common Born–Oppenheimer molecular dynamics (BOMD) method in that the QM electron effect is included in the calculation of energy and forces for the nuclei´s classical motion.[62] However, BOMD acts on the electronic structure problem within the time-independent Schrödinger equation, CPMD explicitly captures the electrons as active degrees of freedom For this purpose, fictitious dynamical variables are used. Core electrons are described by a pseudopotential and valence electrons are described by plane wave basis sets in CPMD simulations. For fixed nuclei, the ground state electronic density is computed self-consistently, utilizing the DFT method. Next, utilizing the electronic density, forces on the nuclei can be approximated for trajectory update.[63]

In BOMD, the wave function of the electrons has to be minimized using the matrix diagonalization at every step. In CPMD, however, the fictitious dynamics relies on the usage of a fictitious electron mass to ensure adiabaticity. The lagrangian is given as:

$$\mathcal{L} = \frac{1}{2}\left(\sum_{I}^{\text{nuclei}} M_I \dot{R}_I^2 + \mu \sum_{i}^{\text{orbitals}} \int dr \left|\dot{\psi}_i(r,t)\right|^2\right) - E[\{\psi_i\},\{R_I\}]$$

where $E[\{\psi_i\}\{R_i\}]$ represents the Kohn-Sham energy density functional that calculates energy values. The orthogonality constraint is given as:

$$\int dr\, \psi_i^*(r,t)\psi_j(r,t) = \delta_{ij}$$

δ_{ij} is the Kronecker delta. The equations of motions are provided by the stationary point of the Lagrangian under variations of ψ_i and R_I, with the orthogonality constraint (see above):

$$M_i R_i = -\nabla_i E\left[[\{\psi_i\}\{R_i\}]\right]$$

$$\boldsymbol{\mu\psi_i(r,t)} = -\frac{\boldsymbol{\delta E}}{\boldsymbol{\delta\psi_i^*(r,t)}} + \sum_{\boldsymbol{J}} \boldsymbol{\Lambda_{ij}\psi_j(r,t)}$$

Complying the orthogonality constraint to $\boldsymbol{\Lambda_{ij}}$ that is a Lagrangian multiplier matrix. CPMD simulations have been conducted to treat larger size transition metal-Aβ complexes with dynamics at the electronic level.

Zn Interactions with Aβ:

Furlan and La Penna successfully linked CPMD simulations of Zn(II):Aβ16 to NMR measurements and presented the results of several initial Zn(II):Aβ16 species.[64] The NMR results for Zn(II):Aβ16 where His6, Glu11, His13 and His14 side chains coordinate to the Zn(II) ion were strongly supported by their studies. Asp1 to Zn(II) coordination drove the complex towards displacement of one of the coordinated His residues. Coordination of Tyr10 to Zn(II) was possible only when Tyr10 was deprotonated. The NMR derived structure with His6, Glu11, His13 and His14 of Aβ16 bonded to Zn is available in the PDB Databank (PDB ID 1ZE9). As structural models with the Asp1, Arg5, Ser8 and Tyr10 side chains coordinated to Zn(II) instead of Glu11 were lacking, the possibility of such models were probed by Furlan and La Penna. To this end, they performed random temperature hybrid Monte Carlo (MC) simulations using the empirical Amber parm94 force field for building the structures with different coordination geometries since the usage of a hybrid MC scheme avoids the occurrence of unstable trajectories as it often happens in high-temperature CPMD simulations based on their and our experiences. Residues 1-16 of Aβ with capped termini were considered in their investigations. They conducted MD simulations and obtained the initial models that had Asp1, Arg5, Ser8, Tyr10 or Glu11 close to the Zn(II) ion along with the His residues. These models were solvated using the TIP3P model for water. MD simulations at 300 K were conducted for 1 to 2 ns for obtaining the structures for CPMD simulations. For the subsequent CPMD simulations, they removed some of the atoms far away from the Zn(II) and conducted them in the gas phase for 1 to 2 ps at 300 K.

Giannozzi *et al.* studied Zn affected structural aggregation characteristics of Aβ by XAS measurements and CPMD simulations.[65] The latter was coupled to various simulation techniques. They constructed four Zn:Aβ models to fit the experimental XAS data. Initial structures were formed by a Zn(II) ion and two Aβ16 peptides. The two Aβ16 peptides with charged N- and C-termini were constructed with backbone dihedral angles set to 180°, and the chains were assembled in an antiparallel fashion with the nitrogen atom of His14 of each chain being coordinated to the Zn(II) ion. The empirical Amber parm94 force field was used for relaxing the structures via MD simulations, by a Monte Carlo simulation where the dihedral angles were randomly varied apart from those belonging to the two His14 side chains that were kept fixed to keep the N(His14)-Zn-N(His14) motif intact. From the obtainedstructures, one particular configuration was picked in which the Zn(II) ion is also close to the N atoms of both His13 residues, as NMR measurements and CPMD simulations had indicated that the N(His13)-N(His14)-Zn-N(His13)-N(His14) coordination is the most stable one. A second model was built in which Zn is coordinated to only three His imidazole rings in a 3N1O fashion. This second model was considered to validate whether a three-imidazole Zn(II) coordination could be an alternative to the four-imidazole Zn(II) coordination proposed in the literature for explaining the XAS data of Zn(II):Aβ. The two Zn(II) ion bridged Aβ16 dimers (models 1 and 2) were truncated to models that were affordable for semiempirical and first principles methods. In fact, residues 1-10 of the peptides were detached and the yielding N-terminus at Glu11 was capped with an acetyl group. The models were placed in an MD cell that was solvated with 376 water molecules (using the TIP3P model for water). The final solvated configurations that were obtained from classical MD simulations were then subjected to tight-binding (TB) semiempirical calculations to relax the systems of interest. After energy minimization using the TB technique, BOMD simulations were performed to bring the systems to room temperature. As from XAS measurements it was suggested that Zn(II) is likely penta-coordinated, the water molecule oxygen atom was closer to Zn(II) at a binding distance as a fifth ligand in both structures. CPMD simulations were then conducted at 300 K using the Vanderbilt ultra-soft pseudopotentials and the Perdew-Burke-Ernzerhof (PBE) exchange correlation function. A third model was designed via slightly modifying the first model by substituting the H atom of one His14 with a second Zn ion. A fourth model was constructed by the addition of aan additional peptide. They found that most stable Zn(II):Aβ complex is the one in which two peptides are bridged by a Zn(II) ion in a four-histidine coordination mode. This model is also compatible with experiments. Another realistic model (model 4) was obtained by the addition of a third peptide to model 3 in a fashion so that Glu11, His14 and a water coordinate to Zn(II). The fourth model not only yielded a very good fit to the XAS data, but also provided the geometric and chemical properties that resulted in both Zn(II) sites as structurally stable.

Cu Interactions with Aβ:

Minicozzi *et al.* conducted CPMD simulations using various models to mimic the interactions between Cu(II) and model Aβ species (see below) in aqueous medium utilizing an explicit water model.[66] They studied the following model systems:

1) Of the amino acid residues 1 to 6, only Asp1, Glu3 and His6 were retained. From the remaining amino acid residues, only His13 and His14 were included in the CPMD simulations. The system was solvated using 125 water molecules. The number of electrons in the system was 1369. Initial metallopeptide configuration was taken from the PDB (code 1ZE9) where Zn(II) was replaced by Cu(II).
2) The backbone of the entire peptide was maintained together with Asp1, His6, Tyr10, Glu11, His13 and His14. The C-terminus was capped again by an $NHCH_3$ group while the N-terminus ended with a NH_2 group. The metallopeptide was solvated using 225 water molecules, yielding 2311 electrons in total. The initial configuration for CPMD was generated from a classical MD simulation of the Cu(II):Aβ16 metallopeptide in water with Cu(II) coordinated to His6, Tyr10, His13 and His14.
3) A similar system as in system 2, but with the Cu(II) coordinating to N-terminus, His6, His13 and His14 was built.

The system involved 223 water molecules and 2295 electrons. The starting configuration for CPMD was generated using classical MD simulation of the Cu(II):Aβ16 peptide in water. In the first model, the nitrogen atom of the N-terminus moved far away from the Cu(II) ion, while the three His residues remained coordinated to the transition metal ion during their simulation time. Therefore, CPMD of the first system yielded results in contrast to NMR measurements that reported the N-terminal nitrogen atom as a coordinating ligand to Cu(II). Next, they investigated whether the N-terminus (second system) or the oxygen atom of Tyr10 (third system) can coordinate to Cu(II). Their simulations were too short for offering a clear perspective on this question. Longer CPMD simulations are needed for studying these systems in detail.

Furlan *et al.* studied several Cu(I):Aβ models and conducted short CPMD simulations (1 ps) and short empirical simulations (3 ns) for gaining insights into the coordination chemistry details of Cu(I) with Aβ.[67] Even though NMR measurements on Cu(I):Aβ16 and Cu(II): Aβ16 gave evidence of for a strong dynamical process, the involvement of all three His residues in the coordination was demonstrated. In order to gain insights into Cu(I) coordination with Aβ, Furlan *et al.* conducted CPMD simulations for various models of Cu(I) coordinated to two or three His residues. Each model was initially built based on hybrid Monte Carlo simulations (see above). The CPMD simulations were performed using 47 to 963 atoms, corresponding to Cu(I) coordination in the smallest truncated model and the full Cu(I):Aβ16 model. Their short-timescale simulations showed that the initial model with three coordinating His residues is not stable as one of the His detaches from Cu(I), leaving only two His residues in the first coordination shell. This result is in accord with XAS experiments but does not agree with NMR experiments. While in the truncated models, an exchange of His14 with His6 occurred, the CPMD simulations of Cu(I):Aβ16 showed that His6 is less likely to be involved in Cu(I) bonding. The dynamic junction between regions 1 to 10 and 11 to 16 of Cu(I):Aβ16 results in the more likely coordination of His13 and His14 rather than the coordination of His6 and His13 to Cu(I). Since Asp1 competes with the His side chains in the solvated model of Cu(II): Aβ, electrostatic forces push Asp1 toward the 1-10/11-16 interface, allowing Asp1 to get close to Cu(II) and eventually stabilizing the oxidized state by coordinating to Cu(II) and thereby replacing His13. A general difference between Cu(I) or Cu(II) coordination with Aβ was reported to be the Cu(II)-induced stretch of the 1-10 region along with a stretch in the 11-16 region of Aβ due to the more preferred binding of His6 and Asp1 when Cu is oxidized, Which is not the case for Cu(I).

La Penna *et al.* studied Cu:Aβ species by CPMD simulations with the goal to gain insights into chemical and physical properties of Cu:Aβ species in the catalysis of the Fenton reaction linked to oxidative stress.[68] The redox behavior of varying coordination geometries was probed considering 8 different models for both monomeric dimeric Cu(II):Aβ with Asp1, His6, His13 and His14 being in the proximity of Cu. An empirical model for monomeric (8 configurations) and dimeric (8 configurations) Aβ16 was utilized for the structure search that satisfied the experimental conditions regarding possible coordination topologies. MC-random walks were performed, followed by candidate configuration selection according to the presence of Asp1, His6, His13 and His14 in the first coordination sphere. The peptide had the DAEFRHDSGYEVHHQK sequence with a charged C-terminus and a neutral N-terminus (NH_2). The overall charge was -3. Selected configurations of the monomeric and dimeric peptides were built by adding a Cu(II) ion as a dummy atom into the coordination sphere center. The Aβ16 peptide was truncated, broken up into two fragments and modified: H_2N-DGGGG-HD-NHMe (with a charge of -2) and Ac-HH-NHMe (with a neutral charge). Asp7 was kept in the model due to the imidazole ring interactions observed earlier (see above). The truncated models were solvated and the systems were neutralized using counterions. MD simulations were performed using an empirical potential. The final geometry was then studied using the CPMD approach. The closest water molecule to the metal was replaced with HO_2^- and copper was reduced to Cu(I). An external force to induce the peroxide resistance against hydroxyl radical production via O-O distance was applied after energy minimization. In all trajectories, they started with His, Asp1 and water molecules in the coordination sphere of Cu(II) since these ligands were shown by experiments to be the most likely ones and are proposed to be active in the redox process. The systems were simulated at 300 K. The resulting trajectories could be divided into three categories. The Fenton-type active trajectories are classified in one class based on 1) Cu being available to water molecules, 2) Cu(I) being coordinated to His and Asp1 in a bent geometry, and 3) a concentrated water rearrangement in the remaining two coordination positions. Class A involved structures with diagonal, non-bent Cu(I) coordination geometry, which stabilized Cu(I) in a fashion so that H_2O_2 did not bind to Cu(I). Class B structures were reported to be potentially redox active and might represent species observed in electrochemistry experiments. Though class B species react slowly with H_2O_2 due to restricted access to Cu(I). Cu:$(Aβ16)_2$ fell to a large extent into class C in comparison to monomeric Cu:Aβ16 that preferred the non-reactive class A. Based on these results, La Penna *et al.* presented a novel mechanism, which could provide insights into the experimentally observed higher reactive oxygen species formed by Cu:Aβ oligomers in comparison to monomers.

In summary, studies on metal-Aβ complexes using first principles simulations usually employed the CPMD technique, which was often linked to empirical molecular simulation techniques. Even though the systems are larger than those studied with the first principles calculations presented in section 2.1 and also intermolecular interactions between solute and solvent as well as the dynamics of the complex are captured, first principles molecular dynamics simulations still cannot treat the full-length disordered metallopeptide in solution. Furthermore, the simulation time scales in most of the studies of metal-Aβ fragments using the CPMD technique is a few picosecond, which is too short for the conformational sampling of Aβ, especially when one considers the dynamic nature of this disordered Aβpeptide.

2.3. Quantum Mechanics/Molecular Mechanics Simulations

Hybrid QM/MM approaches have become a widely used tool for investigating chemical reactions. The system region where the chemical process occurs is treated using quantum chemistry theory (see above), while the rest of the system is treated by molecular mechanics (see below). Most of the schemes can be expressed generally as:

$$E = E_{QM} + E_{QM/MM} + E_{pol} + E_{boundary}$$

The $E_{QM/MM}$ term is the interaction energy between these two regions via ssuming that both regions remain fixed. The E_{pol} term represents the impact of either region changing as a result of the presence of the other region, such as solvent reorganization. The $E_{boundary}$ represents the effect of the rest of the surroundings, such as bulk water. Chemical reactivity can be studied in large systems, such as disordered metal-Aβ systems. The binding of transition metal ions by Aβ can cause polarization, charge transfer effects and coordination geometries, which are not accurately explained using force fields.

Zn Interactions with Aβ:

Furlan and La Penna used NMR measurements and QM/MM simulations and reported ab initio simulation results of several Zn:Aβ16 models.[69] NMR results supported their findings where His6, His13, His14 and Glu11 side chains bind to the Zn(II) ion. Binding of Asp1 to Zn resulted in a complex that showed disconnection of one of the bonded His. Coordination between Zn(II) and Tyr10 occurred when Tyr10 was deprotonated.

Marakov and co-workers studied a small-size model Zn(II) binding site of Aβ using isothermal titration calorimetry experiments and QM/MM simulations.[70] They provided thermodynamic evidence for the region 6-14 as the minimal Zn(II) binding site wherein the metal ion is coordinated to His6, Glu11, His13 and His14. The molecular mechanics approach was applied using the Amber parameters parm99 with corrections provided by Duan *et al*.[71] The QM system was described with DFT in the generalized gradient approximation (GGA) using the PW91 functional. Ultrasoft VDB pseudopotential was used to determine the interactions between valence electrons and ionic cores. Side chain atoms of His6, Glu11, His13, His14 were included in the QM system. The total size of the QM system was 38 atoms. In the case of the Aβ(11-14) fragment, which they also studied, seven water molecules close to zinc were included in QM system as well. Van der Waals interactions were poorly described by default DFT calculations and these were corrected using the Grimme analytical potential.Simulation systems were solvated with water molecules using the TIP4P model for water, and the total charge was neutralized with sodium and chloride ions. The prepared systems were subjected to QM/MM simulations. Temperature coupling was applied using the Noose-Hover scheme, allowing for observing the systems at body temperature. Because ultrasoft pseudopotentials were employed, the valence electrons basis set consisted of plane waves. Overall, they used isothermal titration calorimetry experiments and QM/MM simulations and both tools showed that three of four residues from the 11-14 region contribute to Zn(II) binding and that this binding is associated with dimerization as well.

Kozin *et al*. studied the dimerization mechanism of two Aβ(11-14) fragments with a Zn(II) ion using QM/MM simulations that were supported by surface plasmon resonance biosensing and electrospray mass spectrometry experiments.[72] For this purpose, they investigated two models: i) the Zn(II) ion being coordinated to residues Glu11 and His14 of fragments, ii) Zn(II) being coordinated to His13 and His14 of both fragments. The formation energy for the dimer calculated utilizing the QM/MM approach for the second model was smaller. They thus concluded that the Zn(II) ion is likely chelated by Glu11 and His14 residues and this finding was supported by isothermal titration calorimetry experiments. The same group (Makarov and co-workers) investigated whether phosphorylation of Ser8 promotes the dimerization of Zn(II) bound Aβ using QM/MM simulations augmented with isothermal titration calorimetry, electrospray ionization mass spectrometry and NMR spectroscopy measurements.[73] For this study, they simulated two model systems: i) the phosphate group provides two oxygen atoms for Zn(II) coordination, the 3rd ligand is the N atom of the His6 side chain, and the 4th ligand coordinating to Zn(II) is the carbonyl oxygen of Asp7, ii) the first three ligands are the same as in the first model and the 4th ligand is the carbonyl oxygen of His6. The QM/MM simulations showed that the energies for these two model systems were almost identical, the second model is energetically only slightly preferred. The conclusion was that, in accord with their NMR experiments, both models can exist in solution.

Cu Interactions with Aβ:

Peroxynitrite causes AD and a mechanism was provided by Giacovazzi *et al*.[74] Ascorbate, dioxygen and nitric oxide presence close to Cu: Aβ yields peroxynitire catalytic production in competition to the production of H_2O_2. To this end, an ONIOM approach was utilized to simulate Cu-Aβ. QM layer which included ascorbate, molecular oxygen and nitric oxide, was described at DFT level utilizing the PBE0 functional the lanl2dz basis set. The Universal Force Field was employed for the MM layer. Structures were optimized including frequency calculations to address their nature as minima or transition states, followed by single-point energy calculations capturing water via a polarizable continuum model (C-PCM). For the generation of a low-energy Cu-Aβ structure to be used in QM/MM calculations, classical MD annealing simulations were conducted using the Amber force field (though it is not clear which set of Amber parameters were chosen for this study). The entire reaction mechanism was analyzed. The underlying hypothesis for this approach is that the catalytic site reactivity is faster than conformational changes of the disordered peptide. This study provided the facts for peroxynitrite catalyzation close to Cu: Aβ.

Fe Interactions with Aβ:

Redox activity and oxygen transport is associated with Heme that is a prosthetic group. Heme is linked with Aβ and possesses peroxidase activity. Two binding sites of Aβ are reactive towards heme; residues 1−16, and residues 17−40/42. Spectroscopic measurements propose that ferriheme and Cu(II) bind to

Aβ simultaneously. These findings contradict what is proposed about the nature of copper in Aβ coordination mechanism. Little was known about the binding of heme to Aβ until 2012. Azimi and Rauk successfully presented the binding of Fe(II)-heme and Fe(III)-heme to Aβ by QM/MM simulations in 2012 and 2013, respectively.[75,76] The computations on Aβ−heme were conducted at the MM level with the Amber force field (second generation Amber force field parameters that were reported in 1995) or using the ONIOM approach. B3LYP/6-31G(d) calculations were conducted to validation the statistical mechanics Amber part 4-methylimidazole (MeIm) complex with Fe(II)−heme. Next, MeIm, Fe(II)−heme geometries in their triplet electronic state, and their adduct were calculated at the B3LYP/6-31G(d) level of theory as well. Same theory was used to compute the harmonic frequency analysis for obtaining zero-point vibrational energies and the thermodynamic properties close to the room temperature. Grimme and co-workers` studies were used to estimate the missing dispersion energy via utilizing the DFT-D3 approach. With such a large system, it was not realistic to perform harmonic frequency analysis for all systems. Therefore, energetics were calculated for selected species. Water was modeled using a polarizable continuum model (IEFPCM). Heme coordination to His was calculated. Results indicated a favorability for His13 followed by His6 and His14 (Figure 3). Making it likely that ferroheme is equally distributed among His in the lack of Cu(I). Direct bonding of iron to His is improved by secondary salt bridge formation between the heme carboxylate group and Lys16 and the N-terminus of Aβ or by a combination of H-bonding and hydrophobic interactions (with Asp7 or Phe20 for His6-heme). Such coordination may influence a non-amyloidogenic conformation and reduce the formation of oligomers and fibrils. Their study could not resolve the debates in the literature. The nature of binding of ferriheme (Fe(III)−heme) to Aβ in the presence of Cu(II) is debated. These studies affirm that ferriheme and Cu(II) may bind simultaneously to Aβ. Despite, these studies indicate that Cu(II) coordinates to at least two or three His residues, leaving no room for the heme to coordinate. Using the same methodology, they also studied Fe(III)−heme−Aβ(1-42)−H2O. Coordination of His was investigated. Their results indicated a similar favorability for His13 and His6 coordination. In both cases, bonding of Fe to His is starker by secondary salt bridges between the heme carboxylate groups and Aβ. As before, Azimi and Rauk concluded that the binding may reduce the formation of neurotoxic oligomers and fibrils by stabilizing an Aβ conformation that cannot oligomerize. Based on their calculated reduction potential, the heme-Aβ complex can act as a peroxidase in its Fe(II) and Fe(III) forms, which is in agreement with experiments.

Due to the higher computational cost relative to pure MM simulations, hybrid QM/MM simulations require a careful consideration of balancing computational cost and accuracy. For both types of simulations it is well appreciated that the key challenge is to strike the proper balance between potential energy accuracy and the degree of conformational sampling. Transition metal ion bound Aβ complexes in solution do not adopt stable structures but a large ensemble of structures due to the disordered nature of Aβ. Moreover, the correctness of the simulations can be affected by the location and treatment of the QM and MM region boundaries, the time scale difference between these two regions, and the limitations due to conformational sampling without special sampling techniques.

2.4. Classical Molecular Dynamics Simulations

Modeling of metal-protein interactions: In classical MD simulations, atom and molecule geometries are determined by solving Newton's equations of motion for a system of interacting particles. Forces between the atoms and their potential energies are calculated using interatomic potentials that depend on molecular mechanics force fields. The potential energy of the system is estimated from the molecular structure via a potential function, also known as a force field. These interactions are divided into bonded and non-bonded interactions. Chemical bonds and angles between these bonds are typically modeled using a simple spring model. The rotation about the chemical bond, otherwise termed the dihedral or torsion, is modeled using a sinusoidal wave function to account for the energy differences between staggered and eclipsed conformations. Finally, the van der Waals and electrostatic interactions are typically modeled via a 6-12 Leonard-Jones potential and Coulomb's law, respectively. Thus, the potential function for MD simulations generally has the following form:

$$U = \sum_{bonds} K_r\left(r - r_{eq}\right)^2 + \sum_{angles} K_\theta\left(\theta - \theta_{eq}\right)^2 + \sum_{dihedrals} \frac{V_n}{2}\left[1 + \cos(n\Phi - \gamma)\right] + \sum_{i<j}^{atoms}\left[\frac{A_{ij}}{R_{ij}^{12}} - \frac{B_{ij}}{R_{ij}^{6}}\right] + \sum_{i<j}^{atoms}\frac{q_i q_j}{\varepsilon R_{ij}}$$

While the form of the potential function is often similar, the method used to develop the force field parameters varies and additional terms may be added to improve the accuracy of the resulting force field. As a result, several different force fields for MD simulations are available. The most commonly used force fields for proteins are different versions of the Amber, CHARMM, GROMOS and OPLS-AA force fields.[77-81] For Aβ and other intrinsically disordered proteins it has been shown by various research groups, including by Coskuner and Uversky, Strodel and co-workers, and Derreumaux and co-workers, that the chosen force field parameters largely impact the MD simulation results. CHARMM22*, CHARMM36m and also the most recent Amber force field, Amber99SB-disp have been identified as the force fields producing structural Aβ ensembles that are best in agreement with various experimental observables, mainly obtained from NMR experiments.[82-85] However, none of these force fields has been applied yet for elucidating the effects of transition metal ions on Aβ, which should be addressed by future simulation studies.

Another shortcoming of classical force fields is their inability to correctly model the coordination of ligands to transition metal ions including ligand to metal ion charge transfer

from. To overcome this limitation, varying approaches have been developed. The nonbonded pathway uses electrostatic and vdW parameters to model the interactions between transition metal and the coordinating ligands.[78-88] While this methodology is the easiest one to be included into existing potential functions, the coordination site geometry may not be stable, allowing the metal ion to bind to additional ligands or even exit the coordination site. Furthermore, as we illustrated, simulated metalloprotein structures may be affected based on the choice of the formal or the partial charge model for simulating electrostatic interactions, which in turn are one of the interactions that govern the calculated minimum energy and the related structure. In several studies, geometric constraint parameters were introduced between metal and the protein binding sites to guarantee that the metal endures in the coordination sphere. However, the binding geometry may continue to fluctuate improbably depending on simulation conditions.[85]

An alternative to the bonded models is provided by the nonbonded dummy model that considers the central metal atom as surrounded by dummy atoms whereby each possesses a partial charge.[67,86-97]The dummy model intends to resolve the known issues of nonbonded models and also those of bonded models (see below), which do not allow for the interconversion between different coordination geometries and exchange of coordinating ligands, by providing a nonbonded description capturing electrostatics and structural parameters. While such models were present for other metal ions, none was available for Cu(II) because of the challenges associated with reproducing the Jahn−Teller distortion until Strodel and co-workers presented a nonbonded model.[98,99] They applied the Cu(II) dummy model in MD simulations of enzymes and Aβ (Figure 4).[91] While no problems were encountered when Cu(II) is stably bound in the active site of an enzyme or at ns time-scale, in longer simulations on the microsecond time scale or when enhanced sampling was used, the coordination geometry could not be retained as Cu(II) left the binding site of Aβ and was not able to bind again in a fashion involving one or more His residues (unpublished results).

These issues in classical mechanics can be resolved by using a bonded model, which captures the binding transition metal ion and ligated protein amino acid residues with covalent bonds. This bonded model enables for a more correct coordination sphere geometry representation as well as metal ion confinement in the center. Metal and coordinated amino acid residues are defined by potential functions that depend on force field parameters. MM simulation result accuracy depends on the chosen force field parameters´quality. Force field parameters can be generated using different methods. Bond, angle or dihedral values are varied while we determine the energetics. [100-114] The Hessian matrix using internal coordinates from frequency calculations can be utilized to compute the force constant values.[114-120] Nonetheless, these two methods yield force field parameters depending on the choice of internal coordinates. Thus, different simulation results can be obtained using different choices in internal coordinates. For getting rid of the internal coordinate dependency, Seminario et al. proposed a strategy to generate force field constant parameters from the Hessian matrix based on Cartesian coordinates rather than internal coordinates.[121]

The force constants for the bonded terms of the potential functional are calculated as follows utilizing the Seminario method. In general, force fluctuations acting on atom (A) due to displacement of another atom (B) is given by:

$$[\boldsymbol{\delta F_A}] = -[\boldsymbol{k_{AB}}] \times [\boldsymbol{\delta x_B}] \qquad (1.1)$$

where [k_{AB}] is the 3 x 3 hessian matrix in Cartesian coordinates, which describes atom A and B interactions. Specifically,

$$[k_{AB}] = \begin{bmatrix} \frac{\partial^2 E}{\partial x_A \partial x_B} & \frac{\partial^2 E}{\partial x_A \partial y_B} & \frac{\partial^2 E}{\partial x_A \partial z_B} \\ \frac{\partial^2 E}{\partial y_A \partial x_B} & \frac{\partial^2 E}{\partial y_A \partial y_B} & \frac{\partial^2 E}{\partial y_A \partial z_B} \\ \frac{\partial^2 E}{\partial z_A \partial x_B} & \frac{\partial^2 E}{\partial z_A \partial y_B} & \frac{\partial^2 E}{\partial z_A \partial z_B} \end{bmatrix} \qquad (1.2)$$

The bond force constants can be calculated by equation 1.3:

$$k_{AB} = \sum_{i=1}^{3} \lambda_i^{AB} |u^{AB} \cdot v_i^{AB}| \qquad (1.3)$$

where λ_i^{AB} and v_i^{AB} are the eigenvalues and eigenvectors of the [k_{AB}] matrix and u^{AB} is the unit vector between the two atoms.

The angle bending force constant value between three atoms (A, B, and C in which B is the central atom) can be calculated from the Hessian matrix as a function of the [k_{AB}] and [k_{CB}] interaction matrices. The angle bending force constant is calculated by equation 1.4:

$$\frac{1}{k_q} = \frac{1}{d_{AB}^2 \sum_{i=1}^{3} \lambda_i^{AB} \left| u^{PA} \times v_i^{AB} \right|} + \frac{1}{d_{CB}^2 \sum_{i=1}^{3} \lambda_i^{CB} \left| u^{PC} \times v_i^{CB} \right|} \qquad (1.4)$$

where, $u^{PA} = u^{N} \times u^{AB}$, $u^{PC} = u^{CB} \times u^{N}$, $u^{N} = \frac{u^{CB} \times u^{AB}}{\left| u^{CB} \times u^{AB} \right|}$

d is the distance between two particles. Using this strategy, torsional angle force constant values can be derived and provide torsion energy´s harmonic behavior. The potential energy due to torsional angle would be calculated via equation 1.5:

$$\sum_{torsions} \frac{k_f}{2} \left(f - f_{eq} \right)^2 \qquad (1.5)$$

Electrostatic potential methods, such as the CHarges from ELectrostatic Potentials (CHELP), CHarges from ELectrostatic Potentials using a Grid based method (CHELPG), electrostatic potential (ESP) and restrained electrostatic potential **(**RESP) methods, derive the atomic charges from a least-squares fit of a significant number of points around the molecule of interest to the electrostatic potential of that molecule.[122-126] These methods vary greatly in the choice of points for the potential fit, the density of points for the potential fit, the point exclusion criteria and the atomic van der Waal radii. Furthermore, the RESP method introduces a hyperbolic penalty function in order to prevent charges of buried atoms being less well-determined.

Classical MD studies of metal-Aβ interactions. Several groups have performed standard and enhanced MD simulations to study the effects of metal-ion binding on the structure and dynamics of monomeric and oligomeric Aβ. The most often used simulation method for enhancing the sampling of Aβ configurations is the replica exchange molecular dynamics (REMD) method, where several MD simulations, the so-called replicas, are run in parallel but at different temperatures or using different potential functions (aka. Hamiltonians).[127-129,131] In the replicas at higher temperatures or with reduced inter-atomic interactions the system can cross energy barriers more easily so that a larger conformational space is sampled. Due to the exchange of conformations between the replicas with a certain probability according to the Metropolis criterion, the target replica, i.e. the replica at the temperature of interest or with the unmodified potential function also explores a larger conformational space. As the REMD method is an enhanced sampling method that does not require a predefined reaction coordinate, it has become very popular for the study of Aβ, whose disordered nature makes it (almost) impossible to define a reaction coordinate.

Zn or Cu Interactions with Aβ:

Li *et al*. conducted replica exchange molecular dynamics (REMD) simulations utilizing the Amber ff03 force field for the protein and the generalized Born (GB) model for the solvent.[130] They simulated the apo and holo Aβ peptide for studying the impacts of Zn(II) binding on the structural distributions of the Aβ(1-40) peptide. The active site of the human carbonic anhydrase II was simulated using the nonbonded parameters of Zn(II) using the molecular orbital method by Hoops and co-workers. Bond constraints were added between Zn(II) and its coordinating atoms according to experimental data, i.e., the His N atoms in His6, His13 and His14 and the Glu11 carboxylate group oxygen atom. The REMD simulation involved 28 replicas. The configurations from these simulations were used to extract the conformational distributions. They reported that the conformational distribution of the Aβ monomer could change with zinc binding. In comparison to the metal free Aβ, the holo-peptide sampled more β-strand structure for CHC and increased probabilities of the Asp23-Lys28 salt bridge and the turn comprising residues 23-28. Since these local structures are essential for Aβ aggregation, the observed effects of zinc binding indicate that the metal causes conformational changes of the monomer that is associated with one of the available mechanisms for the metal ion affected aggregation of Aβ.

Miller *et al*. studied the coordination of Zn(II) to an Aβ42 complex comprising eight peptides and considered following stoichiometries: 8 Zn(II)-8 Aβ42 and 4 Zn(II)-8 Aβ42.[131] The initial structures were taken from the Aβ17-42 Lührs model (PDB ID: 2BEG). They used the CHARMM27 parameters for the peptide and the TIP3P model for the solvent. For obtaining the relative structural stabilities and populations of the Zn(II)-Aβ1-42 oligomers, the conformations from the last 5 ns were taken and the solvation energies of these systems were calculated using the implicit solvation method Generalized Born using Molecular Volume (GBMV). The total time of their MD simulation remains unknown. They also performed REMD simulations on these systems - after MD simulations for evaluating free energy surfaces based on potential of mean force calculations. The starting structures for the REMD simulations were from prior standard MD simulations, i.e. simulations without special sampling methods. They effect of Zn(II) on Aβ structures was studied. They linked covalently the structures from experiments. They noticed that, for the Zn(II)-Aβ42 oligomer, Zn(II) can bind intra- and inter-molecularly, forming a dimer. The solvation energy of Zn(II)-Aβ42 oligomers decreases and therefore enhances aggregation propensity. The β-sheet association around the C-terminal hydrophobic region is not affected significantly upon Zn(II) binding. Antiparallel and other ordered structures are pronounced but parallel β-sheet structure formation is still most abundant. Their REMD simulations further supported an experimental observation and led to the conclusion that increasing Zn(II) concentration could reduce the aggregation kinetics, however, the aggregation kinetics are much faster than in metal-free solution.

Wise-Scira *et al*. used REMD simulations to investigate the structures and thermodynamic properties of Zn(II):Aβ40 and Zn(II):Aβ42 monomers in an aqueous solution environment (Figure 5).[132] Seminario´s strategy was utilized for calculating the model Zn:His_3Glu moiety force constant values. For calculating the electrostatic interaction parameters, the same group conducted partial charge calculations using the B3LYP/6-31G*//B3LYP/6-31G* method. The starting Zn:Aβ40 and Zn:Aβ42 structures were prepared by connecting the NMR-derived Zn:Aβ16 structure (PDB ID: 1ZE9) with the Leu17–Val40 and Leu17–Ala42 fragments, respectively. Simulations were performed using the Amber ff99SB parameters and the Onufriev–Bashford–Case generalized Born implicit solvent model. The impact of inter-molecular interactions between the solute and solvent molecules were not captured in this study. Their results showed distinct characteristics for the two metallopeptide alloforms. For example, prominent β-sheet formation in the N-terminal region of Zn:Aβ40 was significantly decreased or lacking in Zn:Aβ42 (Figure 6). Their findings indicate that blocking multiple residues important for forming abundant β-sheet structure, which are located in the central hydrophobic core and C-terminal regions of Aβ42, via antibodies or small organic molecules might help to reduce the aggregation of Zn(II)-bound Aβ42.

Zn(II) is not stably bound to Aβ and exhibits a fast ligand exchange kinetics. Experiments suggest that Zn(II) promotes aggregation through inter-molecular bridges forming Zn:$(Aβ)_2$ species. Pan and Patterson conducted MD simulations on Zn:Aβ and Zn:$(Aβ)_2$ with varying combinations of coordinating ligands including His6, His13, His14 and Glu11 as suggested by previous QM calculations and NMR measurements.[133] In the study by Pan and Patterson, the force field parameters for the metal-ligand bonds were predicted from DFT calculations. Hessian matrix was used along with the vibrational frequency data to obtain force constant values for the Zn-ligand species and were included in CHARMM22 force field parameters. The residues His6, His13, His14 and Glu11 were covalently bound to the metal as reported by NMR measurements via utilizing the force constant values obtained from QM

calculations. For the metal-dimer species, DFT calculation results showed that the 2 Glu and 2 His residues and 4 His residues are relatively stable dimeric cross linkages at neutral pH. There were different possible dimeric structures considering symmetric coordination of the two Aβ peptides. They used all-atom simulations with explicit water solvent (TIP3P) and the CHARMM22/CMAP force field augmented with their Zn(II) parameters. Simulations showed that zinc causes conformational changes in Aβ. Moreover, zinc reduces the helix content and increases the disorder degree of the peptide. β-sheet formation was observed prominently at the C-terminus in Zn:Aβ and Zn:$(Aβ)_2$ complexes. This study suggested that Zn-binding to Aβ accelerates Aβ aggregation.

Recent developments of bifunctional molecules, which interact with Aβ and metal ions supply promising therapeutics to AD. Traditional metal chelating agents, such as ethylenediaminetetraacetic acid (EDTA), clioquinol (CQ), an analog of clioquinol (PBT2), and cyclen, have already been utilized as therapeutic agents to disrupt metal-Aβ interactions. Some molecules like CQ and PBT2 have been shown to improve the cognition behavior by reducing the amount of plaque deposits in phase II clinical trials. However, the adverse side effects limit their long-term use. The molecular mechanism of how Aβ interacts with small molecules in the presence or absence of metal ions is still elusive. Due to the dynamic nature and polymorphic states of Aβ, it is rather difficult to capture the binding sites of small compounds through *in vitro* experiments. Theoretical studies also face great challenges because the time scale required for conformational changes induced by small molecules is still far beyond the accessible computation time in terms of the ''induced fit'' hypothesis of protein–ligand interactions . An alternative hypothesis termed conformational selection has emerged based on experimental results, which assumes that the ligand first selects the most favored preexisting conformations of a protein, and then the binding interactions lead to redistribution of the relative conformations in solution (population shift). Xu et al. combined conformational sampling and selection to identify the binding mode of zinc-bound Aβ with three different small-size bifunctional molecules using a conformational selection model, REMD simulations and docking calculations.[134] The bifunctional molecules exhibit their dual functions by first preferentially interfering with hydrophobic residues 17–21 and/or 30–35 of Zn(II)-bound Aβ. Interactions caused by Zn(II) surrounding residues may disrupt metal and Aβ interactions. Their binding free energy calculations further demonstrate that Aβ and bifunctional molecule interactions were governed by enthalpy rather than entropy. It should be noted that entropy calculations for monomers and oligomers of intrinsically disordered proteins in solution still provide a challenge to the theoretical and computational chemistry society.[125]

Han et al. modeled Zn and Cu binding to Alzheimer's Aβ peptide considering Tyr10, His6, His13 and His14 as coordinating ligands involved and using the Aβ(10-21) fragment.[136] As force field Amber parm96 was used together with the TIP3P model for water. The MD protocol included an equilibration part lasting for 5 ps and a production part of 0.5 ps at a temperature of 298K. Each 0.1 ps a configuration was saved, leading to five configurations, which were further energy-minimized prior analysis. Based on their results, the N atom of the imidazole ring of His14, the O atom of a backbone carbonyl groups and two O atoms from water occupy the four ligand positions of the monomeric complex, while in the aggregated form of Aβa His13(N)–metal–His14(N) bridge was formed. However, their simulations are too short for predicting the structures accurately.

Parthasarathy *et al*. conducted solid-state NMR measurements along with MD simulations for investigating Cu(II)-binding to Aβ40 fibrils.[137] Amber ff99sb force field with generalized Born (GB) implicit solvation were utilized. However, Jahn-Teller effects were ignored in this study and accurate force field parameters for Cu(II):Aβ were not developed using QM calculations. Their experiments demonstrated small changes upon Cu(II) coordination and demonstrated that Met35 might not be oxidized through Cu in fibrils. The MD simulations confirmed the binding sites suggested by the NMR results and the stability of such Cu(II) binding. Furthermore, the coexistence of a variety of Cu(II)-binding modes unique to Aβ fibrils was indicated from the simulations that are realized by both intra- and inter-molecular contacts and highly concentrated coordination sites due to the in-register parallel β-sheet arrangements.

Jiao and Yang studied Cu(II):Aβ using MD simulations and the Aβ(10-21) fragment instead of the full-size Aβ40/Aβ42 peptide.[138] The ESFF force field parameters along with the SPC model for water was used. For each MD simulation, equilibration time was 1 ns, followed by 1 ns of data collection for analysis. Based on their short simulations without special sampling techniques, they reported that a tri-ring 4N coordination mode of the Cu(II):Aβ complexes occurred where the $N_δ$ atom of histidine acts as anchor site and its adjacent backbone N atoms as essential coordination sites forming the equatorial plane. They concluded that Cu(II):Aβ coordination is against the formation of stable fibrils, i.e. that Cu(II) inhibits the aggregation of Aβ into fibrils. However, the coordination geometry must be predefined in their simulations.

Mantri *et al*. studied whether Cu(II) binds to Aβ40 and Aβ42 in the same fashion.[129] They first conducted B3LYP/6-31G** calculations where Cu(II) was modeled by the LACVP basis set on model Cu(II):ligand systems for obtaining bonded force field parameters, which were used for a subsequent long scale MD simulations. The resulting trajectories were analyzed for clustering using the Jarvis–Patrick algorithm, and evaluation of the energy-minimized representative provided the copper–peptide complex stability. They evaluated the relative energies of different isomeric structures and found that Aβ40 and Aβ42 possess varying binding modes, suggesting that shorter Aβ fragments truncated at the C-terminus may not be realistic models.

Boopathi and Kolandaivel conducted MD simulations of Zn(II)- and Cu(II)-bound Aβ40 and Aβ42 monomers in water.[140] However, the choice of transition metal-Aβ force field parameters for simulating Zn(II):Aβ and Cu(II):Aβ were not mentioned in their study, which suggests that they used a simple nonbonded model. OPLS-AA parameters were used for the protein and the TIP3P model for water was chosen in their MD simulations. As they did not conduct enhanced sampling MD

simulations, the conformational sampling of Aβ is limited. They reported that Zn(II):Aβ40 adopts a β-hairpin structure, which was promoted by the turn region in the mid domain region and increases the hydrophobic contact between the CHC and the C-terminal regions. The turn region was stabilized by alternative salt-bridges. The same β-hairpin structure was reported to be not stable in Zn(II):Aβ42 due to the absence of these salt-bridges.

Coskuner compared the structures of Zn(II)-bound Aβ40 and Aβ42 to those of Cu(II)-bound Aβ40 and Aβ42 in aqueous solution utilizing REMD simulations.[141] To simulate the Cu:Aβ40 and Cu(II):Aβ42 alloforms using a bonded model for the Cu:Aβ moiety, they developed the force field parameters for the Cu(II):$(His)_3$Glu species utilizing full-length models and extensive first principles calculations. Different sets of REMD simulations were conducted using the Amber ff99SB parameters for the rest of Aβ. The Onufriev–Bashford–Case generalized Born implicit solvent model was utilized. 16 replicas were utilized. Conformational Gibbs free energies were calculated using the MM/PBSA method (Table 1). Their results demonstrated that copper binding to both Aβ alloforms is thermodynamically less preferred than zinc binding, which is in agreement with experiments.[131] Moreover, Cu(II) binding impacts the thermodynamic properties, secondary and tertiary structural properties of Aβ40 and Aβ42 different than Zn(II) binding. Coskuner-Weber also investigated the impact of different coordination chemistries on the structures and thermodynamic properties of Cu(II):Aβ40 and Cu(II):Aβ42 in an aqueous solution environment. To this end, the force field parameters of Cu(II):$(His)_3$Asp, Cu(II):$(His)_3$Glu and Cu(II):$(His)_3$Tyr were developed using the Seminario method as described above. Amber ff99SB parameters and the Onufriev-Bashford-Case generalized Born implicit solvent model were used in REMD simulations. The correlation between simulation and experiment was judged based on C_α and H_α chemical shift values for the Aβ42 peptide in aqueous solution. Experimental data (NMR) was obtained from Prof. Michael Zagorski (Figure 7).[143] The thermodynamic properties of apo- and Cu(II)-bound Aβ40 and Aβ42 revealed that the Cu(II)-bound structures are less preferred than apo-Aβ40 and apo-Aβ42 in aqueous solution. Additionally, both Aβ alloforms favored different structures based on the coordination chemistry. Specifically, the thermodynamic preference for the coordination sites is in the order Cu:$(His)_3$Glu11 < Cu:$(His)_3$Tyr10 < Cu: $(His)_3$Asp1 for both Aβ alloforms. The free energy surfaces of the free and Cu(II)-bound Aβ peptides also revealed that the conformational ensemble of the Aβ peptides is altered by Cu(II) coordination and that the change in the conformational ensemble differs based on the chosen binding site. In general, the helical content of the Cu(II)-bound alloforms decreases upon Cu(II) binding in the N-terminal and CHC regions for all three coordination chemistries (Figure 8). The β-sheet content is decreased for the Cu(II):Aβ40 peptide except within residues Leu34-Val40. Conversely, the Aβ42 peptide shows a boost in β-sheet content in the CHC and C-terminal regions for all three binding sites and also in the N-terminal region for the Cu:$(His)_3$Glu11 binding site. Furthermore, the increased structuring in the C-terminal region of the free Aβ42 in comparison to the free Aβ40 is still observed when Cu(II) binds to the peptide. Additionally, increased structuring in the CHC region due to β-sheet formation for the Cu(II)-bound Aβ42 peptides as to the Cu(II)-bound Aβ40 peptides is also observed. These β-sheet content variations indicate that the Cu(II)-coordinated Aβ peptides have an increased aggregation tendency in comparison to the free Aβ peptides and that the Cu(II)-bound Aβ42 peptides will aggregate more rapidly than the Cu(II)-bound Aβ40 peptides. Intrinsic aggregation propensity calculation revealed that the CHC and C-terminal regions are most likely to be involved in the aggregation of the free and Cu(II)-bound Aβ40 and Aβ42 peptides in aqueous solution, which is further enhanced by Cu(II) binding for the CHC region of Aβ40 and for both the CHC and C-terminal regions of Aβ42.

Li and co-workers studied the impacts of Cu(II) binding on the structures of monomeric and dimeric Aβ using MD simulations in 2016.[138] They used the CPMD-derived structures for Cu(II):ligands complexes that were obtained by La Penna and co-workers (see above) and used the Seminario method for calculating the force field parameters of the Cu(II):ligands complex for conducting classical MD simulations. They used the AMBER force field 99SB for the rest of the protein and the TIP3P model for water in their simulations. They obtained the force field parameters for Cu(II) bound to His6, His13 (or His14) and Asp1 with distorted planar geometry. They demonstrated that upon Cu(II) binding, the β-sheet content of Aβ is reduced. This was in accord with experiments. In addition, one possible mechanism for amorphous assembly is that the Asp23-Lys28 salt bridge, which plays a crucial role in β-sheet formation, becomes more dynamic upon Cu(II) ion binding to the Aβ peptide´s N-terminus. Based on their findings, Cu(II) coordination delays Aβ dimerization process as observed by experiments. The reported mechanism is associated with slow formation of inter-chain salt bridges in dimer as well as with decreased hydrophobicity of monomer upon Cu(II) binding.

Strodel and co-workers studied the impact of Cu(II) binding on Aβ42 monomers and dimers using Hamiltonian replica exchange molecular dynamics (H-REMD) simulations (Figure 9).[133,134] The initial structure of the Cu(II): Aβ42 complex was built by combining the Cu(II): Aβ16 model proposed by Alí-Torres *et al*.[46] (see above) and the structure of Aβ(17-42) as determined by NMR spectroscopy for full-length Aβ42 in a hexafluoroisopropyl alcohol/water mixture (PDB ID 1Z0Q).[144] For modeling the Cu(II):Aβ42 binding site, they first developed force-field parameters for usage with OPLS-AA for Cu(II) ligated by His6 and His13 and the amine and carbonyl groups of Asp1 in a distorted square-planar geometry. To this end, they conducted DFT calculations at the B3LYP/def2-TZVP level with D3 dispersion correction on a truncated model including Cu(II) and the coordinating residues. OPLS-AA and TIP4P parameters were used. In addition to the Cu(II): Aβ42 system they also investigated the effect of varying pH values (5.3, 6.0, and 7.4) on Aβ42 structures and thermodynamics elucidated by the transition network approach, which Strodel and co-workers developed for capturing the structural dynamics and aggregation of Aβ. It was found that a charge reduction of Aβ42 either provoked by Cu(II) binding or by mild acidic conditions leads to an increased β-sheet formation, which might promote aggrega-

tion. However, Cu(II) complexation also increased the structural flexibility of Aβ42 despite more β-sheets being present in Aβ42.[133] Similar observations were made in their study of the Cu(II)-bridged Aβ2 dimer where the Cu(II) ion was coordinated by a pair of His13 and His14 residues from the two Aβ42 peptides.[134] Based on MP2 and DFT calculations a set of OPLS-AA force field parameters was developed to describe the interactions between Cu(II) and the Aβ42 dimer, which were used in H-REMD simulations with 24 replicas, OPLS-AA as force protein force field, and TIP4P as water model. The Hamiltonian scaling factors applied to Cu(II):(Aβ42)2 were exponentially distributed between 1.0 and 0.4. Each replica was simulated for 500 ns and the last 400 ns of the replica with the unmodified potential were used for analysis. In addition to Cu(II) binding, Strodel and co-workers studied the effects of different external conditions on the conformations of the Aβ42 dimer: at pH 7.4 representing physiological conditions, at pH 5.3 representing acidic conditions linked to brain inflammation, and an oxidized Aβ42 dimer containing two C_α-centered Gly25 radicals as a result of oxidative stress. As for the monomer,[133] transition networks were calculated from the H-REMD simulations, which revealed that the decreased pH considerably and Cu(II) binding slightly increased the β-sheet content. Moreover, Cu(II) binding increased the exposed hydrophobic surface area, which together with an increased β-sheet formation can contribute to an increased oligomerization propensity and toxicity. Interestingly the increase in β-sheet content as induced by either a mild acidic pH or Cu(II) binding is accompanied by an increase in peptide flexibility, especially in the C-terminal half of the peptides. This was an unexpected finding as the general assumption is that structure formation and conformational flexibility reduction go hand in hand, suggesting that intrapeptide diffusion also plays a role during amyloid formation. The effects of oxidized Gly25 was rather limited on the Aβ42 dimer, indicating that oxidative stress, while being important in the pathology of AD, has no direct influence on the structural and aggregation properties of Aβ.

La Penna and Li used metadynamics MD simulations on a system composed of two Aβ(1-42) peptides and a Cu(II) ion in aqueous solution.[134] They used the Amber 99SB parameters and the TIP3P model for water. For the Cu(II):ligand complex, the Seminario method was used (see above). They used different models; Cu is coordinated to Asp1 (N and O), His6, His13 (same peptide); Cu is bound to Asp1 and His6 (one peptide) and His13 (second peptide). Their study illustrated that the superoxide production is related to low-energy intermediates after a high-energy Cu(I): Aβ complex formation. Despite the bias for high-energy reduced reactant species, the reduction of Cu(II): Aβ product by superoxide can also occur as demonstrated in Ref. 134.

It was shown that curcumin (CUA), a polyphenolic phytochemical, inhibits the aggregation of Aβ. The joint interactions of Aβ with metal ions and CUA were not clear until Kozmon and Tvaroska conducted MD simulations including Aβ42, Cu(II) and CUA at the same time.[135] For this purpose, the CUA structure was generated and optimized at the B3LYP/6-31+G(d) level, which was then used to generate force field parameters by the antechamber tool, where RESP charges and gaff parameters were employed. The Cu(II) ion was treated using the non-bonded approach, which only considers to the metal ion as van der Waals sphere with electrostatics. Different interaction modes between Aβ, CUA and Cu(II) were investigated. Their results showed that CUA or a higher concentration of Cu(II) ions impact the conformations of Aβ42. Furthermore, calculations of the Aβ42 complex with CUA and Cu(II) ions showed that CUA can chelate the Cu(II) ion and directly interacts with Aβ.

One of the early clinical trials for treating AD was done with clioquinol (CQ), an old drug that was used to treat fungal and protozoal infections and also acts as a zinc and copper chelator. It can dissolve amyloid aggregates by forming stable chelation with metal ions. A drawback of CQ is its poor aqueous solubility, making it hard to reach the fibrils and thus enter the protein interior. Benzothiazole is known to possess a strong binding affinity for Aβ plaques and has been used as imaging agent for Aβ plaques. Geng *et al*. synthesized three compounds, (E)-2-((benzo[d]-thiazol-2-ylimino)methyl)phenol (CQ1), (E)-2-((benzo[d]thiazol-2-ylimino)methyl)-4-chlorophenol (CQ2),and (E)-2-((benzo[d]-thiazol-2-ylimino)methyl)-4-nitrophenol (CQ3), as the new inhibitors of Cu(II)-Aβ aggregation, where CQi (i=1,2,and 3) is the collective term for them.[136] Experiments revealed that the three CQi compounds possess a high efficiency for both Cu(II) elimination and Aβ assembly inhibition at pH=6.6. The mechanisms of both aggregation inhibition for these compounds was obscure, especially its pH dependence. To answer this question, Dong *et al*. simulated the interactions between the CQi drugs and Cu(II)-Aβ40 monomers at two pH values.[137] The Amber parm94 force field parameters were used for the rest of the protein along with the TIP3P model for water for simulating the solvent. They reported the binding free energies for CQi with monomeric Cu(II):Aβ40 in water. Regarding binding strength, CQ2 was shown to be the best compound. As the special role of D23 in both Aβ aggregation and stabilizing the Aβ fibril, the generation of H-bond between CQ3 and D23 of Aβ40 peptide is believed to be responsible to CQ3 the strongest disaggregation capacity.

Fe Interactions with Aβ:

Boopathi and Kolandaivel studied Zn(II):Aβ, Cu(II):Aβ and Fe(II):Aβ using MD simulations and provided a comparison of these metallopeptide structures.[130,139] For these simulations, optimized truncated Zn(II):$(His)_3$, Cu(II):$(His)_3$ and Fe(II):$(His)_3$ structures, i.e., without a fourth ligand binding to the metal ions, were generated at the M06-2X/ 6-311++G(2df,2pd)+LANL2DZ level of theory and used to derive OPLS-AA parameters for these coordination sites. They were then used to set up the full Zn(II):Aβ, Cu(II):Aβ and Fe(II):Aβ systems, which were solvated in TIP3P water and their dynamics studied using 200 ns MD simulations. They reported that Fe(II) binding reduces the helical structures and increases the β-sheet content, indicating that Fe(II) binding promotes the aggregation of the disordered peptide into amyloid structures.

Manganese Interactions with Aβ:

Mn(II) is the oxidation state that is most stable for manganese, and it has paramagnetic properties. For low pH values it was found that Mn(II) does not contribute to Aβ aggregation. Additionally, Bush *et al*. found in a Zn(II) competitive assay with APP that Mn(II) competed off Zn(II) to approximately the same extent as Cd(II), Pb(II), Al(III), Hg(II) and Cu(II) did in its toxicity.[140] In a study using Mn(II) ions as paramagnetic probes in Aβ/micelle conglomerates evidence was found for an Mn(II) binding specificity for the N-terminus of Aβ.[141,142] Wallin *et al*. conducted MD simulations along with NMR, CD, and fluorescence spectroscopies as well as AFM measurements to study the binding of Mn(II) to Aβ.[142] As starting point for their MD simulations the NMR structure (PDB ID 1ZEQ) of Aβ16 bound to a Zn(II) ion with His6, His13, His14 and Glu11 as ligands was used. The Zn(II) atom in the original structure was replaced with an octahedral Mn(II) dummy model, which was developed as part of this study. OPLS-AA parameters were used for Aβ, which was solvated utilizing the TIP4P model for water. These joint simulations and experiments proposed that Mn(II) binds only weakly to Aβ, which likely does not have a large effect on the disordered nature of the peptide and its aggregation into amyloid fibrils.

3. CONCLUSIONS

We have summarized recent studies that used different computational chemistry approaches for studying the binding between transition metal ions and Aβ and the resulting impacts on the structures, thermodynamic properties and aggregation propensities of monomeric and oligomeric Aβ in aqueous solution. Experiments face challenges in elucidating time- and atom-resolved details of the binding and effects of transition metal ions on Aβ, but so do computational chemistry studies for different reasons. Extensive efforts went into computational chemistry studies of transition metals with monomeric or oligomeric Aβ, from which various coordination geometries for the metal-Aβ binding were proposed. While these different coordination mechanisms might all occur due to the disordered and dynamic nature of Aβ, it seems that the binding of Glu11, Asp1 or Tyr10 along with three His residues are the most preferred.

The studies of transition metals binding to Aβ requires both quantum and classical mechanics or their hybrid version. Quantum level studies do not allow studying the full-size metallopeptide in solution and can also not capture the highly dynamic nature of the transition metal binding to Aβ and the dynamics of this peptide in solution. Even though useful insights have been gained from quantum level studies with or without short-time (i.e., picosecond time scale) dynamics, these also led to a debate regarding the coordination modes of transition metal ions with Aβ as different studies produced different coordination geometries. An additional shortcoming of the hybrid QM/MM simulations is that their accuracy depends on the location and treatment of the boundary between the QM and MM regions, the time scale difference between these two regions, and the limitations due to limited conformational sampling. Classical MD simulations provided insights into the full-size structures and thermodynamic properties of transition metal ion bound Aβ in solution, especially when long-time simulations (on the microsecond time scale) or special sampling techniques were used. However, these simulations depend on force field parameters. A particular problem of classical MD simulations of metallopeptides is the description of the coordination between the transition metal ions and the binding residues. Even though nonbonded, dummy and bonded models have been developed to overcome this issue, the resulting force field parameters for the metal ion: Aβ complex do not capture the impacts of polarization nor do they accurately represent the partially filled d orbitals that would allow the study of different coordination geometries. Furthermore, the description of the different bonding types (particularly π bonding) between biomolecules and metal ions is difficult within classical molecular simulations.

Moreover, it is well known that the chosen force field parameters impact the predicted structures and thermodynamic properties of Aβ. While most protein force fields nowadays provide balanced and reliable descriptions for folded proteins, this is less the case for intrinsically disordered proteins, such as Aβ. Therefore, we also expect a force field dependence of the results for transition metal ion bound Aβ; however, this remains to be investigated. Due to the difficulties of experiments in elucidating thermodynamic and kinetic details for monomeric and oligomeric Aβ due to its highly dynamic and aggregation-prone nature, the force field developments are affected as well since there is only limited experimental data to which the outcome from computational chemistry studies of Aβ can be compared to. The lack of reliable simulation results in turn impacts the development of new experimental approaches in this area. Therefore, the goal remains that the physics, chemistry and biology of transition-metal bound, disordered Aβ complexes needs to be fully elucidated.

Nevertheless, transition metals may coordinate in a heterogeneous manner to various ligands due to the highly dynamic and disordered nature of Aβ and the *in vivo* environment may also affect these coordination chemistries. For each possible coordination scenario, computational chemistry studies provided insights into the mechanism, structural and thermodynamic properties. Given these information, metal ion chelators or small chemical/biological drugs can be synthesized for finding a cure for AD, whose pathology is affected by transition metal ions.

REFERENCES

1. K. J. Barnham and A. I. Bush, Metals in Alzheimer´s and Parkinson´s diseases, *Curr. Opin. Chem. Biol.* 2008, 12(2):222-228.

2. G. Perry, A. D. Cash, M. A. Smith, Alzheimer Disease and Oxidative Stress, *J. Biomed. Biotech*. 2002, 2(3):120-123.

3. C. J. Maynard, A. I. Bush, C. L. Masters, R. Cappai, Q.-X. Li, Metals and amyloid-β in Alzheimer's disease, *Int. J. Exp. Pathol.* 2005, 86(3):147-159.

4. P. A. Adlard and A. I. Bush, Metals and Alzheimer's disease, *J. Alz. Dis.* 2006, 10(2-3):145-163.

5. M. A. Lovell, J. D. Robertson, W. J. Teesdale, J. L. Campbell, W. R. Markesbery, Copper, iron and zinc in Alzheimer's disease senile plaques, *J. Neurol. Sci.* 1998, 158(1):47-52.

6. M. A. Deibel, W. D. Ehmann, W. R. Markesbery, Copper, iron, and zinc imbalances in severely degenerated brain regions in Alzheimer's disease: possible relation to oxidative stress, *J. Neurol. Sci.* 1996, 143(1-2):137-142.

7. A. I. Bush, The metallobiology of Alzheimer's disease, *Trends Neurosci*. 2003, 26(4):207-214.

8. Y. H. Hung, A. I. Bush, R. A. Cherny, Copper in the brain and Alzheimer's disease, *J. Biol. Inorg. Chem.* 2010, 15(1):65-7.

9. K. J. Barnham, C. L. Masters, A. I. Bush, Neurodegenerative diseases and oxidative stress, Nature Rev. Drug. Discov. 2004, 3, 205-214.

10. D. A. Loeffler, J. R. Connor, P. L. Juneau, B. S. Snyder, L. Kanaley, A. J. DeMaggio, H. Nguyen, C. M. Brickman, P. A. LeWitt, Transferrin and Iron in Normal, Alzheimer's Disease, and Parkinson's Disease Brain Regions, *J. Neurochem.* 1995, 65(2):710-716.

11. O. Wise-Scira, L. Xu, G. Perry, O. Coskuner, Amyloid-β peptide structure in aqueous solution varies with fragment size, *J. Chem. Phys.* 2011, 135(20):205101.

12. J. Hardy and D. J. Selkoe, The Amyloid Hypothesis of Alzheimer's Disease: Progress and Problems on the Road to Therapeutics, *Science*, 2002, 297(5580):353-356.

13. A. E. Roher, M. O. Chaney, Y.-M. Kuo, S. D. Webster, W. B. Stine, L. J. Haverkamp, A. S. Woods, R. J. Cotter, J. M. Tuohy, G. A. Krafft, B. S. Bonnell, M. R. Emmerling, Morphology and Toxicity of Aβ-(1-42) Dimer Derived from Neuritic and Vascular Amyloid Deposits of Alzheimer's Disease, *J. Biol. Chem.* 1996, 271, 20631-20635.

14. C. Haass and D. J. Selkoe, Soluble protein oligomers in neurodegeneration: lessons from the Alzheimer's amyloid β-peptide, *Nature Rev. Mol. Cell Biol.* 2007, 8, 101-112.

15. M. Sakono and T. Zako, Amyloid oligomers: formation and toxicity of Aβ oligomers, *FEBS J.* 2010, 1348-1358.

16. I. Benilova, E. Karran, B. De Strooper, The toxic Aβ oligomer and Alzheimer's disease: an emperor in need of clothes, *Nature Neurosci.* 2012, 15, 349-357.

17. M. Stefani, Structural features and cytotoxicity of amyloid oligomers: Implications in Alzheimer's disease and other diseases with amyloid deposits, *Prog. Neurobiol.* 2012, 99(3):226-245.

18. J. P. Clearly, D. M. Walsh, J. J. Hofmeister, G. M. Shankar, M. A. Kuskowski, D. J. Selkoe, K. H. Ashe, Natural oligomers of the amyloid-β protein specifically disrupt cognitive function, *Nature Neurosci*. 2005, 8:79-84.

19. G. S. Bloom, Amyloid-β and Tau The Trigger and Bullet in Alzheimer Disease Pathogenesis, *JAMA Neurol.* 2014, 71(4):505-508.

20. I.-C. Stancu, B. Vasconcelos, D. Terwel, I. Dewachter, Models of β-amyloid induced Tau-pathology: the long and "folded" road to understand the mechanism, *Mol. Neurodeg.* 2014, 9:51.

21. J. Danielsson, R. Pierattelli, L. Banci, A. Gräslund, High-resolution NMR studies of the zinc-binding site of the Alzheimer's amyloid β-peptide, *FEBS J.* 2006, 274(1):46-59.

22. L. Hou and M. G. Zagorski, NMR Reveals Anomalous Copper(II) Binding to the Amyloid Aβ Peptide of Alzheimer's Disease, *J. Am. Chem. Soc.* 2006, 128(29):9260-9261.

23. C. Talmard, L. Guilloreau, Y. Coppel, H. Mazarguil.

P. Faller, Amyloid-Beta Peptide Forms Monomeric Complexes With CuII and ZnII Prior to Aggregation, *ChemBIOChem.* 2007, 8(2):163-165.

24. N. G. Nair, G. Perry, M. A. Smith, P. V. Reddy, NMR Studies of Zinc, Copper, and Iron Binding to Histidine, the Principal Metal Ion Complexing Site of Amyloid-β Peptide, *J. Alz. Dis.,* 2010, 20(1):57-66.

25. F. Bousejra-ElGarah, C. Bijani, Y. Coppel, P. Faller, C. Hureau, Iron(II) Binding to Amyloid-β, the Alzheimer's Peptide, *Inorg. Chem*. 2011, 50(18):9024-9030.

26. C. D. Syme nd J. H. Viles, Solution 1H NMR investigation of Zn2+ and Cd2+ binding to amyloid-beta peptide (Aβ) of Alzheimer's disease, *Biochim. Biophys. Acta Prot. Proteom.* 2006, 1764(2):246-256.

27. P. Faller and C. Hureau, Bioinorganic chemistry of copper and zinc ions coordinated to amyloid-β peptide, *Dalton Trans.* 2009, 1080-1094.

28. V. Minicozzi, F. Stellato, M. Comai, M. D. Serra, C. Ptorich, W. Meyer-Klaucke, S. Morante, Identifying the Minimal Copper- and Zinc-binding Site Sequence in Amyloid-β Peptides, *J. Biol. Chem.* 2008, 283:10784-10792.

29. P. Dorlet, S. Gambarelli, P. Faller, C. Hureau, Pulse EPR Spectroscopy Reveals the Coordination Sphere of Copper(II) Ions in the 1–16 Amyloid-β Peptide: A Key Role of the First Two N-Terminus Residues*, Ang. Chem. Int. Ed*. 2009, 48(49):9273-9276.

30. C. Hureau, V. Balland, Y. Coppel, P. L. Solari, E. Fonda, P. Faller, Importance of dynamical processes in the coordination chemistry and redox conversion of copper amyloid-β complexes, *J. Biol. Inorg. Chem.* 2009, 14(7):995-1000.

31. T. Kowalik-Jankowska, M. Ruta, K. Wiśniewska, L. Lankiewicz, Coordination abilities of the 1–16 and 1–28 fragments of β-amyloid peptide towards copper(II) ions: a combined potentiometric and spectroscopic study, *J. Inorg. Biochem.* 2003, 4(1):270-282.

32. J. Shearer, P. E. Callan, T. Tran, V. A. Szalai, Cu K-edge X-ray absorption spectroscopy reveals differential copper coordination within amyloid-β oligomers compared to amyloid-β monomers, *Chem. Comm.* 2010, 46, 9137-9139.

33. J. H. Viles, Metal ions and amyloid fiber formation in neurodegenerative diseases. Copper, zinc and iron in Alzheimer's, Parkinson's and prion diseases, *Coord. Chem. Rev.* 2012, 256(19-20):2271-2284.

34. D. Jiang, X. Li, R. Williams, S. Patel, L. Men, Y. Wang, F. Zhou, Ternary Complexes of Iron, Amyloid-β, and Nitrilotriacetic Acid: Binding Affinities, Redox Properties, and Relevance to Iron-Induced Oxidative Stress in Alzheimer's Disease, *Biochem.* 2009, 48(33):7939-7947.

35. B. Allies, A. Cote-Daban, S. Sayen, F. Collin, I. Kieffer, E. Guillon, P. Faller, C. Hureau, Zinc(II) Binding Site to the Amyloid-β Peptide: Insights from Spectroscopic Studies with a Wide Series of Modified Peptides, Inorg. Chem., 2016, 55, 10499.

36. P. Cui, Y. Wang, W. Chu, X. Guo, F. Yang, M. Yu, H. Zhao, Y. Dong, Y. Xie, W. Gong, Z. Wu, How Water Molecules Affect the Catalytic Activity of Hydrolases-A XANES Study of the Local Structures of Peptide Deformylase, Sci. Rep. 2014, 4, 1-6.

37. O. Coskuner and V. N. Uversky, Alanine Scanning Effects on the Biochemical and Biophysical Properties of Intrinsically Disordered Proteins: A Case Study of the Histidine to Alanine Mutations in Amyloid-β42, J. Chem. Inf. Mod. 2019, 59, 871.

38. C. Hureau, P. Dorlet, Coordination of redox active metal ions to the amyloid precursor protein and to amyloid-β peptides involved in Alzheimer disease. Part 2: Dependence of Cu(II) binding sites with Aβ sequences, Coord. Chem. Rev. 2012, 256, 2175.

39. C. Hureau, Coordination of redox active metal ions to the amyloid precursor protein and to amyloid-β peptides involved in Alzheimer disease. Part 1: An overview, Coord. Chem. Rev. 2012, 256, 2164.

40. O. Wise-Scira, L. Xu, T. Kitahara, G. Perry, O. Coskuner, Amyloid-β peptide structure in aqueous solution varies with fragment size, 2011, 135(20), 205101.

41. J. W. Karr, V. A. Szalai, Cu(II) Binding to Monomeric, Oligomeric, and Fibrillar Forms of the Alzheimer's Disease Amyloid-β Peptide, Biochem., 2008, 47, 5006.

42. T. C. Allison, O. Coskuner, C. A. Gonzalez, Metallic Systems: A Quantum Chemist´s Perspective, CRC Press, Taylor & Francis, ISBN: 978-1-4200-6077-5.

43. K. J. Barnham, F. Haeffner, G. D. Giccotosto, C. C. Curtain, D. Tew, C. Mavros, K. Beyreuther, D. Carrington, C. L. Masters, R. A. Cherny, R. Cappai, A. I. Bush, Tyrosine gated electron transfer is key to the toxic mechanism of Alzheimer's disease β-amyloid, *FASEB J*, 2004, 18(12):1427-1429.

44. O. Coskuner and V. N. Uversky, Tyrosine Regulates β-Sheet Structure Formation in Amyloid-β42: A New Clustering Algorithm for Disordered Proteins, *J. Chem. Inf. Mod.* 2017, 57(6):1342-1358.

45. T. Prosdocimi, L. De Gioia, G. Zampella, L. Bertini, On the generation of OH· radical species from H2O2 by Cu(I) amyloid beta peptide model complexes: a DFT investigation, *J. Biol. Inorg. Chem.* 2016, 21(2):197-212.

46. S. Zirah, S. A. Kozin, A. K. Mazur, A. Blond, M. Cheminant, I. Segalas-Milazzo, P. Debey, S. Rebuffat, Structural changes of region 1-16 of the Alzheimer disease amyloid β-peptide upon zinc binding and in vitro aging, *J. Biol. Chem.* 2006, 281, 2151–2161.

47. E. Gaggelli, Z. Grzonka, H. Kozlowski, C. Migliorini, E. Molteni, D. Valensin, G. Valensin, Structural features of the Cu(II) complex with the rat Aβ(1-28) fragment, *Chem. Commun.* 2008, 341–343.

48. E. Gaggelli, H. Kozlowski, D. Valensin, G. Valensin, Copper Homeostasis and neurodegenerative disorders (Alzheimer's, prion, and Parkinson's diseases and amyotrophic lateral sclerosis), *Chem. Rev.,* 2006, 106, 1995–2044.

49. T. Marino, N. Russo, M. Toscana, M. Pavelka, On the metal ion (Zn2+, Cu2+) coordination with beta-amyloid peptide: DFT computational study, *Interdiscip. Sci. Comput. Life Sci.* 2010, 2, 57.

50. V. A. Streltsov, S. J. Titmuss, V. C. Epa, K. J. Barnham, C. L. Masters, J. N. Varghese, The Structure of the Amyloid-β Peptide High-Affinity Copper II Binding Site in Alzheimer Disease, *Biophys. J.* 2008, 95(7):3447-3456.

51. O. Coskuner-Weber, Revisiting Cu(II) Bound Amyloid-β40 and Amyloid-β42 Peptides: Varying Coordination Chemistries. *Journal of the Turkish Chemical Society, Section A: Chemistry* 2018, 5(3):981-1008.

52. A. Mirats, J. Ali-Torres, L. Santiago-Rodriguez, M. Sodupe, G. La Penna, Dioxygen activation in the Cu-amyloid β complex, *Phys. Chem. Chem. Phys.* 2015, 17:27270-27274.

53. J. Ali-Torres, J-D. Marechal, L. Rodriguez-Santiago, M. Sodupe, Three Dimensional Models of Cu2+-Aβ(1–16) Complexes from Computational Approaches, J. Am. Chem. Soc. 2011, 133, 15008-15014.

54.. T. Miura, K. Suzuki, H. Takeuchi, Binding of iron(III) to the single tyrosine residue of amyloid β-peptide probed by Raman spectroscopy, *J. Mol. Struct.* 2001, 598(1):79-84.

55. M. Nakamura, N. Shishido, A. Nunomura, M. A. Smith, G. Perry, Y. Hayashi, K. Nakayama, T. Hayashi, Three Histidine Residues of Amyloid-β Peptide Control the Redox Activity of Copper and Iron, *Biochem.* 2007, 46(44):12737-12743.

56. J. Ali-Torres, L. Rodriguez-Santiago, M. Sodupe, A. Rauk, Structures and Stabilities of Fe2+/3+ Complexes Relevant to Alzheimer's Disease: An ab Initio Study, *J. Phys. Chem. A* 2011, 115(45):12523-12530.

57. K. J. Barnham, V. B. Kenche, G. D. Ciccotosto, D. P. Smith, D. J. Tew, X. Liu, K. Perez, G. A. Cranston, T. J. Johanssen, I. Volitakis, A. I. Bush, C. L. Masters, A. R. White, J. P. Smith, R. A. Cherny, R. Cappai, Platinum-based inhibitors of amyloid-β as therapeutic agents for Alzheimer's disease, *Proc. Natl. Acad. Sci.* 2008, 105(19):6813-6818.

58. V. A. Streltsov, E. V. Chandana, S. A. James, Q. I. Churches, J. M. Caine, V. B. Kenche, K. J. Barnham, Structural insights into the interaction of platinum-based inhibitors with the Alzheimer's disease amyloid-β peptide, *Chem. Commun.* 2013, 49(97):11364-11366.

59. E. Fermi, Motion of neutrons in hydrogenous substances, *Ricerca Scientifica* 1936, 7:13-52.

60. H. Hellmann, A New Approximation Method in the Problem of Many Electrons, *J. Chem. Phys.* 1935, 3, 61.

61. R. Car and M. Parrinello, Unified Approach for Molecular Dynamics and Density-Functional Theory, *Phys. Rev. Lett.* 1985, 55(22):2471-2474.

62. M. Born and J. R. Oppenheimer, On the Quantum Theory of Molecules, *Annalen der Physik* 1927, 389(20):457-484.

63. L. Verlet, Computer "Experiments" on Classical Fluids. I. Thermodynamical Properties of Lennard-Jones Molecules, *Phys. Rev.* 1967, 159, 98.

64. S. Furlan and G. La Penna, Modeling of the Zn2+ binding in the 1–16 region of the amyloid β peptide involved in Alzheimer's disease, *Phys. Chem. Chem. Phys.* 2009, 11, 6468-6481.

65. P. Giannozzi, K. Jansen, G. La Penna, V. Minicozzi, S. Morante, G. Rossid, F. Stellato, Zn induced structural aggregation patterns of β-amyloid peptides by first-principle simulations and XAS measurements, *Metallomics* 2012, 4, 156-165.

66. V. Minicozzi, S. Morante, G. C. Rossi, F. Stellato, N. Christian, K. Jansen, The role of metals in amyloid aggregation—Experiments and ab initio simulations, *Int. J. Quant. Chem.* 2008, 108(11):1992-2015.

67. S. Furlan, C. Hureau, P. Faller, G. La Penna, Modeling the Cu+ Binding in the 1−16 Region of the Amyloid-β Peptide Involved in Alzheimer's Disease, *J. Phys. Chem. B* 2010, 114(46):15119-15133.

68.G. La Penna, C. Hureau, O. Andreussi, P. Faller, Identifying, By First-Principles Simulations, Cu[Amyloid-β] Species Making Fenton-Type Reactions in Alzheimer's Disease, *J. Phys. Chem. B* 2013, 117(51):16455-16467.

69. S. Furlan and G. La Penna, Modeling of the Zn2+ binding in the 1–16 region of the amyloid β peptide involved in Alzheimer's disease, *Phys. Chem. Chem. Phys.* 2009, 11, 6468-6481.

70. P. O. Tsvetkov, A. A. Kulikova, A. V. Golovin, Y. V. Tkachev, A. I. Archakov, S. A. Kozin, A. A. Makarov, Minimal Zn(2+) binding site of amyloid-β *Biophys. J.* 2010, 99(10):L84-L86.

71. Y. Duan, C. Wu, S. Chowdhury, M. C. Lee, G. Xiong, W. Zhang, R. Yang, P. Cieplak, R. Luo, T. Lee, J. Caldwell, J. Wang, and P. Kollman, A point-charge force field for molecular mechanics simulations of proteins based on condensed-phase quantum mechanical calculations. *J. Comput. Chem.* 2003 24:1999-2012.

72. S. A. Kozin, Y. V. Mezentsev, A. A. Kulikova, M. A. Indeykina, A. V. Golovin, A. S. Ivanov, P. O. Tsvetkov, A. A. Makarov, Zinc-induced dimerization of the amyloid-β metal-binding domain 1–16 is mediated by residues 11–14, *Mol. Biosyst.* 2011, 7, 1053-1055.

73. A. A. Kulikova, P. O. Tsvetkov, M. I. Indeykina, I. A. Popov, S. S. Zhokhov, A. V. Golovin, V. I. Polshakov, S. A. Kozin, E. Nudlerf, A. A. Makarov, Phosphorylation of Ser8 promotes zinc-induced dimerization of the amyloid-β metal-binding domain, *Mol. Biosyst.* 2014, 10, 2590-2596.

74. R. Giacovazzi, I. Ciofini, L. Rao, C. Amatorea, C. Adamo, Copper–amyloid-β complex may catalyze peroxynitrite production in brain: evidence from molecular modeling, *Phys. Chem. Chem. Phys.* 2014, 16, 10169-10174.

75. S. Azimi and A. Rauk, The Binding of Fe(II)–Heme to the Amyloid Beta Peptide of Alzheimer's Disease: QM/MM Investigations, *J. Chem. Theory Comp.* 2012, 8(12):5150-5158.

76. S. Azimi and A. Rauk, Fe(III)–Heme Complexes with the Amyloid Beta Peptide of Alzheimer's Disease: QM/MM Investigations of Binding and Redox Properties of Heme Bound to the His Residues of Aβ(1–42), *J. Chem. Theory Comp.* 2013, 9(9):4233-4242.

77. W. D. Cornell, P. Cieplak, C. I. Bavly, I. R. Gould, K. M. Merz, D. M. Ferguson, D. C. Spellmeyer, T. Fox, J. W. Caldwell, P. A. Kollman, A second generation force field for the simulation of proteins, nucleic acids, and organic molecules, *J. Am. Chem. Soc.* 1995, 117(9):5179-5197.

78. V. Hornak, R. Abel, A. Okur, B. Strockbine, A. Roitberg, C. Simmerling, Comparison of multiple amber force fields and development of improved protein backbone parameters, *Prot. Struct. Funct. Bioinf.* 2006, 65(3):712-725.

79. B. R. Brooks, R. E. Bruccoleri, B. D. Olafson, D. J. States, S. Swaminathan, M. Karplus, CHARMM: A program for macromolecular energy, minimization, and dynamics calculations, *J. Comp. Chem.* 1983, 4(2):187-217.

80. M. Christen, P. H. Hünenberger, D. Bakowies, R. Baron, R. Bürgi, D. P. Geerke, T. N. Heinz, M. A. Kastenholz, V. Krautler, C. Osstenbrink, The GROMOS software for biomolecular simulation: GROMOS05, *J. Comp. Chem.* 2005, 26(16):1719-1751.

81. G. A. Kaminski, R. A. Friesner, J. Tirado-Rives, W. L. Jorgensen, Evaluation and reparametrization of the OPLS-AA force field for proteins via comparison with accurate quantum chemical calculations on peptides, *J. Phys. Chem. B* 2001, 105(28):6474-6487.

82. O. Coskuner-Weber and V. N. Uversky, How accurate are your simulations? Effects of confined aqueous volume and AMBER FF99SB and CHARMM22/CMAP force field parameters on structural ensembles of intrinsically disordered proteins: Amyloid-β42 in water, *Intrinsically Disord. Prot.* 2017, 5(1):e1377813.

83. M. Carballo-Pacheco and B. Strodel, Comparison of force fields for Alzheimer's A β42: A case study for intrinsically disordered proteins, *Prot. Sci.* 2016, 26(2):174-185.

84. P. H. Nguyen, M. S. Li, P. Derreumaux, Effects of all-atom force fields on amyloid oligomerization: replica exchange molecular dynamics simulations of the Aβ16–22 dimer and trimer, *Phys. Chem. Chem. Phys.* 2011,13, 9778-9788.

85. V. H. Man, P. H. Nguyen, P. Derreumaux, High-Resolution Structures of the Amyloid-β 1–42 Dimers from the Comparison of Four Atomistic Force Fields, *J. Phys. Chem. B* 2017, 121(24):5977-5987.

86. C. R. Watts, A. Gregory, C. Frisbie, S. Lovas, Effects of force fields on the conformational and dynamic properties of amyloid β(1-40) dimer explored by replica exchange molecular dynamics simulations, *Prot. Struct. Func. Bioinf.* 2018, 86(3):279-300.

87. M. D. Smith, J. S. Rao, E. Segelken, L. Cruz, Force-Field Induced Bias in the Structure of Aβ21-30: A Comparison of OPLS, AMBER, CHARMM, and GROMOS Force Fields, *J. Chem. Inf. Mod.* 2015, 55(12):2587-2595.

88. A. R. Bizzarri, C. X. Wang, W. Z. Chen, S. Cannistraro, Hydrogen bond analysis by MD simulation of copper plastocyanin at different hydration levels, *Chem. Phys.* 1995, 201(2-3):463-472.

89. F. Ryvkin and F. T. Greenway, A peptide model of the copper-binding region of lysyl oxidase, *J. Inorg. Biochem.* 2004, 98(8):1427-1435.

90. Q. Wang, N. H. Werstiuk, J. R. Kramer, R. A. Bell, Effects of Cu Ions and Explicit Water Molecules on the Copper Binding Domain of Amyloid Precursor Protein APP(131-189): A Molecular Dynamics Study, *J. Phys. Chem. B*, 2011, 115(29):9224-9235.

91. R. H. Stote and M. Karplus, Zinc Binding in Proteins and Solution – A Simple but Accurate Nonbonded Representation, *Prot.* 1995, 23(1):12-31.

92. R. B. Wu, Z. Y. Lu, Z. X. Cao, Y. K. Zhang, A Transferable Nonbonded Pairwise Force Field to Model Zinc Interactions in Metalloproteins, *J. Chem. Theory Comp.* 2011, 7(2):433-443.

93. W. F. Li, J. Zhang, J. Wang, W. Wang, Metal-coupled folding of Cys(2)His(2) zinc-finger, *J. Am. Chem. Soc.* 2008, 130(3):892-900.

94. E. G. Brandt, M. Hellgren, T. Brinck, T. Bergman, O. Edholm, Molecular dynamics study of zinc binding to cysteines in a peptide mimic of the alcohol dehydrogenase structural zinc site, *Phys. Chem. Chem. Phys.* 2009, 11(6):975-983.

95. M. Hodak, R. Chisnell, W. Lu, J. Bernholc, Functional implications of multistage copper binding to the prion protein, *Proc. Natl. Acad. Sci.* 2009, 196(28):11576-11581.

96. N. J. Deng, L. Yan, D. Singh, P. Cieplak, Molecular basis for the Cu2+ binding-induced destabilization of beta 2-microglobulin revealed by molecular dynamics simulation, *Biophys. J.* 2006, 90(11):3865-3879.

97. Y. P. Pang, Novel zinc protein molecular dynamics simulations: Steps toward antiangiogenesis for cancer treatment, *J. Mol. Mod.* 1999, 5(10):196-202.

98. Y. P. Pang, K. Xu, J. El Yazal, F. G. Prendergast, Successful molecular dynamics simulation of the zinc-bound farnesyltransferase using the cationic dummy atom approach, *Prot. Sci.* 2000, 9(10):1857-1865.

99. Q. Liao, S. C. L. Kamerlin, B. Strodel, Development and Application of a Nonbonded Cu2+ Model That Includes the Jahn–Teller Effect, *Phys. Chem. Lett.* 2015, 6(13):2657-2662.

100. Q. H. Liao, A. Pabis, B. Strodel, S. C. L. Kamerlin, Extending the Nonbonded Cationic Dummy Model to Account for Ion-Induced Dipole Interactions, *J. Phys. Chem. Lett.* 2017, 8(21):5408-5414.

101. Q. Liao, M. C. Owen, O. O. Olubiyi, B. Barz, B. Strodel, Conformational Transitions of the Amyloid-β Peptide Upon Copper(II) Binding and pH Changes, *Isr. J. Chem.* 2017, 57(7-8):771-784.

102. J. Sabolovic, C. S. Tautermann, T. Loerting, K. R. Liedl, Modeling anhydrous and aqua copper(II) amino acid complexes: A new molecular mechanics force field parametrization based on quantum chemical studies and experimental crystal data, *Inorg. Chem.* 2003, 42(7):2268-2279.

103. M. Mentler, A. Weiss, K. Grantner, P. del Pino, D. Deluca, S. Fiori, C. Renner, W. M. Klaucker, L. Moroder, U. Bertsch, H. A. Kretzschmar, P. Tavan, F. G. Parak, A new method to determine the structure of the metal environment in metalloproteins: investigation of the prion protein octapeptide repeat Cu2+ complex, *Eur. Biophys. J. Biophys. Lett.* 2005, 34(2):97-112.

104. P. Comba and R. Remenyi, A new molecular mechanics force field for the oxidized form of blue copper proteins, *J. Comp. Chem.* 2002, 23(7):697-705.

105. S. D. Dalosto, Computer simulation of the interaction of Cu(I) with Cys residues at the binding site of the yeast metallochaperone Cu(I)-Atx1, *J. Phys. Chem. B*, 2007, 111(11):2932-2940.

106. Y. Zhu, Y. Su, X. Li, Y. Wang, G. Chen, Evaluation of AMBER force field parameters for copper(II) with pyridylmethyl-amine and benzimidazolylmethyl-amine ligands: A quantum chemical study, *Chem. Phys. Lett.* 2008, 455(4-6):354-360.

107. B. T. O. Holt and K. M. Merz, Insights into Cu(I) exchange in HAH1 using quantum mechanical and molecular simulations, *Biochem.* 2007, 46(30):8816-8826.

108. N. A. Veldhuis, M. J. Kuiper, R. C. J. Dobson, R. B. Pearson, J. Camakaris, In silico modeling of the Menkes copper-translocating P-type ATPase 3rd metal binding domain predicts that phosphorylation regulates copper-binding, *Biometals*, 2011, 24(3):477-487.

109. E. S. Riihimaki, J. M. Martinez, L. Kloo, Molecular dynamics Simulations of Cu(II) and the PHGGGWGQ octapeptide, *J. Phys. Chem. B*, 2007, 111(35):10529-10537.

110. R. J. F. Branco, P. A. Fernandes, M. J. Ramos, Molecular dynamics simulations of the enzyme Cu, Zn superoxide dismutase, *J. Phys. Chem. B* 2006, 110(33):16754-16762.

111. A. Vedani and D. W. Huhta, A New Force-Field for Modeling Metalloproteins, *J. Am. Chem. Soc.* 1990, 112(12):4759-4767.

112. K. M. Merz, CO2 Binding to Human Carbonic Anhydrase-II, *J. Am. Chem. Soc.* 1991, 113(2):406-411.

113. S. C. Hoops, K. W. Anderson, K. M. Merz, Force-Field Design for Metalloproteins, *J. Am. Chem. Soc.* 1991, 113(22):8262-8270.

114. M. A. L. Eriksson, T. Hard, L. Nilsson, Molecular Dynamics Simulations of the Glucocorticoid Receptor DNA-Binding Domain in Complex with DNA and Free in Solution, *Biophys. J.* 1995, 68(2):402-426.

115. J. Bredenberg and L. Nilsson, Modeling zinc sulfhydryl bonds in zinc fingers, *Int. J. Quant. Chem.* 2001, 83(3-4):230-244.

116. D. Qui, S. Dasgupta, P. Kozlowski, W. A. Goddard, T. G. Spiro, Chromophore-in-protein modeling of the structures and resonance Raman spectra for type 1 copper proteins, *J. Am. Chem. Soc.* 1998, 120(49):12791-12797.

117. D. Qui, L. T. Kilpatrick, N. Kitajima, T. G. Spiro, Modeling Blue Copper Protein Resonance Raman-Spectra with Thiolate-Cu(Ii) Complexes of a Sterically Hindered Tris(Pyrazolyl)Borate, *J. Am. Chem. Soc.* 1994, 116(6):2585-2590.

118. J. O. A. de Kerpel and U. Ryde, Protein strain in blue copper proteins studied by free energy perturbations, *Prot.* 1999, 36(2):157-174.

119. D. Suarez and K. M. Merz, Molecular dynamics simulations of the mononuclear zinc-beta-lactamase from Bacillus cereus, *J. Am. Chem. Soc.* 2001, 123(16):3759-3770.

120. T. Tuccinardi, A. Martinelli, E. Nuti, P. Carelli, F. Balzano, G. Uccello-Barretta, G. Murphy, A. Rossello, Amber force field implementation, molecular modelling study, synthesis and MMP-1/MMP-2 inhibition profile of (R)and (S)-N-hydroxy-2-(N-isopropoxybiphenyl-4-ylsulfonamido)-3-methylbutanamid es, *Bioorg. Med. Chem.* 2006, 14(12):4260-4276.

121. J. M. Seminario, Calculation of intramolecular force fields from second-derivative tensors, *Int. J. Quant. Chem.* 1996, 60(7):1271-1277.

122. U. C. Singh and P. A. Kollman, An Approach to Computing Electrostatic Charges for Molecules, *J. Comp. Chem.* 1984, 5(2):129-145.

123. L E. Chirlian and M. M. Francl, Atomic Charges Derived from Electrostatic Potentials-A Detailed Study, *J. Comp. Chem.* 1987, 8(6):894-905.

124. B. H. Besler, K. M. Merz, P. A. Kollman, Atomic Charges Derived From Semiempirical Methods, *J. Comp. Chem.* 1990, 11(4):431-439.

125. C. M. Breneman and K. B. Wiberg, Determining Atom-Centered Monopoles From Molecular Electrostatic Potentials - The Need For High Sampling Density In Formamide Conformational-Analysis, *J. Comp. Chem.* 1990, 11(3):361-373.

126. C. I. Bavly, P. Cieplak, W. D. Cornell, P. A. Kollman, A Well-Behaved Electrostatic Potential Based Method Using Charge Restraints For Deriving Atomic Charges - The RESP Model, *J. Phys. Chem.* 1993, 97(40):10269-10280.

127. D. E. Earl and M. W. Deem, Parallel Tempering: Theory, Applications, and New Perspectives, *Phys. Chem. Chem. Phys.* 2005, 7:3910.

128. Y. Sugita and Y. Okamoto, Replica-Exchange Molecular Dynamics Method For Protein Folding, *Chem. Phys. Lett.* 1999, 314:141-151.

129. M. N. Radford, Sampling From Multimodal Distributions Using Tempered Transitions, *Stat. Comput.* 1996, 6(4):353-366.

120. W. Li, J. Zhang, Y. Su, J. Wang, M. Qin, W. Wang, Effects of Zinc Binding on the Conformational Distribution of the Amyloid-β Peptide Based on Molecular Dynamics Simulations, *J. Phys. Chem. B* 2007, 111(49):13814-13821.

121. Y. Miller, B. Ma, R. Nussinov, Zinc ions promote Alzheimer Aβ aggregation via population shift of polymorphic states, *Proc. Natl. Acad. Sci.* 2010, 107(21):9490-9495.

122. O. Wise-Scira, L. Xu, G. Perry, O. Coskuner, Structures and free energy landscapes of aqueous zinc(II)-bound amyloid-β(1–40) and zinc(II)-bound amyloid-β(1–42) with dynamics, *J. Biol. Inorg. Chem.* 2012, 17(6):927-938.

123. L. Pan and J. C. Patterson, Molecular Dynamics Study of Zn(Ab) and Zn(Ab)2, *PLOS One* 2013, 8(9):e70681.

124. L. Xu, K. Gao, C. Bao, X. Wang, Combining conformational sampling and selection to identify the binding mode of zinc-bound amyloid peptides with bifunctional molecules, *J. Comp.-Aided Mol. Des.,* 2012, 26(8):963-976.

125. O. Coskuner and O. Wise-Scira, Arginine and Disordered Amyloid-β Peptide Structures: Molecular Level Insights into the Toxicity in Alzheimer's Disease, *ACS Chem. Neurosci.* 2013, 4(12):1549-1558.

126. D. Han, H. Wang, P. Yang, Molecular modeling of zinc and copper binding with Alzheimer's amyloid β-peptide, *BioMetals*, 2008, 21(2):189-196.

127. S. Parthasarathy, F. Long, Y. Miller, Y. Xiao, D. McElheny, K. Thurber, B. Ma, R. Nussinov, Y. Ishii, Molecular-Level Examination of Cu2+ Binding Structure for Amyloid Fibrils of 40-Residue Alzheimer's β by Solid-State NMR Spectroscopy, *J. Am. Chem. Soc.* 2011, 133(10):3390-3400.

128. Y. Jiao and P. Yang, Mechanism of Copper(II) Inhibiting Alzheimer's Amyloid β-Peptide from Aggregation: A Molecular Dynamics Investigation, *J. Phys. Chem. B*, 2007, 111(26):7646-7655.

129. Y. Mantri, M. Fioroni, M.-H. Baik, Computational study of the binding of CuII to Alzheimer's amyloid-β peptide: Do Aβ42 and Aβ40 bind copper in identical fashion?, *J. Biol. Inorg. Chem.* 2008, 13(8):1197-1204.

130. S. Boopathi and P. Kolandaivel, Role of zinc and copper metal ions in amyloid β-peptides Aβ1–40 and Aβ1–42 aggregation, *RSC Adv*., 2014, 4, 38951-38965.

131. O. Coskuner, Divalent copper ion bound amyloid-β(40) and amyloid-β(42) alloforms are less preferred than divalent zinc ion bound amyloid-β(40) and amyloid-β(42) alloforms, *J. Biol. Inorg. Chem.* 2016, 21(8):957-973.

133. Q. Liao, M. C. Owen, S. Bali, B. Barz, B. Strodel, Aβ under stress: the effects of acidosis, Cu2+-binding, and oxidation on amyloid β-peptide dimers, *Chem. Comm.* 2018, 54:7766-7769.

134. G. La Penna, M. S. Li, Towards High-Throughput Modelling of Copper Reactivity Induced by Structural Disorder in Amyloid Peptides, Chem. European J. 2018, 24(20):5259-5270.

135. S. Kozmon and I. Tvaroska, Molecular dynamic studies of amyloid-beta interactions with curcumin and Cu2+ ions, *Chem. Papers* 2015, 69(9):1262-1276.

136. J. Geng, M. Li, L. Wu, J. Ren, X. Qu, Inhibition of metal-induced amyloid aggregation using light-responsive magnetic nanoparticle prochelator conjugates, *J. Med. Chem.* 2012, 55:9146-9155.

137. M. Dong, H. Li, D. Hu, W. Zhao, X. Zhu, H. Ai, A Molecular Dynamic Study on the Inhibition Mechanisms of Drugs CQ1-3 to the Alzheimer A#40 Aggregation induced by Cu, *ACS Chem. Neurosci.* 2016, 7(5):599-614.

138. P. D. Q. Huy, Q. V. Vuong, G. La Penna, P. Faller, M. S. Li, Impact of Cu(II) Binding on Structures and Dynamics of Aβ42 Monomer and Dimer: Molecular Dynamics Study, *ACS Chem. Neurosci.* 2016, 7(10):1348-1363.

139. S. Boopathi and P. Kolandaivel, Fe(2+) binding on amyloid β-peptide promotes aggregation, *Prot.* 2016, 84(9):1257-1274.

140. A. I. Bush, G. Multhaup, R. D. Moir, T. G. Williamson, D. H. Small, B. Rumble, P. Pollwein, K. Beyreuther, C. L. Masters, A novel zinc(II) binding site modulates the function of the beta A4 amyloid protein precursor of Alzheimer's disease, *J. Biol. Chem.* 1993, 268(22):16109-16112.

141. J. Jarvet, J. Danielsson, P. Damberg, M. Oleszczuk, A. Graslund, Positioning of the Alzheimer Aβ(1-40) peptide in SDS micelles using NMR and paramagnetic probe, *J. Biomol. NMR* 2007, 39:63-72.

142. C. Wallin, Y. S. Kulkarni, A. Abelein, J. Jarvet, Q. Liao, B. Strodel, L. Olsson, J. Luo, J. P. Abrahams, S. B. Sholts, P. M. Roos, S. C. L. Kamerlin, A. Graslund, S. K. T. S. Warmlander, Characterization of Mn(II) ion binding to the amyloid-β peptide in Alzheimer´s disease, *J. Trace Elem. Med. Biol.* 2016, 38:183-193.

143. L. Hou, H. Shao, Y. Zhang, H. Li, N. K. Menon, E. B. Neuhaus, J. M. Brewer, I. –J. L. Byeon, D. G. Ray, M. P. Vitek, T. Iwashita, R. A. Makula, A. B. Przybyla, M. G. Zagorski, Solution NMR Studies of the Aβ(1−40) and Aβ(1−42) Peptides Establish that the Met35 Oxidation State Affects the Mechanism of Amyloid Formation, *J. Am. Chem. Soc.* 2004, 126(7):1992-2005.

144. S. Tomaselli, V. Esposito, P. Vangone, N. A. J. van Nuland, A. M. J. J. Bonvin, R. Guerrini, T. Tancredi, P. A. Temussi, D. Picone, The α-to-β Conformational Transition of Alzheimer's Aβ-(1–42) Peptide in Aqueous Media is Reversible: A Step by Step Conformational Analysis Suggests the Location of β Conformation Seeding, *ChemBioChem.* 2006, 7(2):257-267.

145. O. Wise and O. Coskuner, New force field parameters for metalloproteins I: Divalent copper ion centers including three histidine residues and an oxygen-ligated amino acid residue, *J. Comp. Chem.* 2014, 35(17):1278-1289.

Table 1: Different models for Zn(II):Aβ proposed from experiments. Taken from Ref. 35.

Fragment/Peptide	Experimental conditions	Proposed binding sites	Refs.
Aβ(1-16)	1 mM in phosphate buffer 50 mM. pH 7.1 (H_2O/D_2O, 9/1), 293 K.	His6, His13, His14, ?	1
Aβ(1-16), Aβ(1-28)	~ 0.1 mM in D_2O, pH 7.8, 293 K	NH_2 (Asp1), His6, His13, His14	2
Aβ(1-40)	50 μM in phosphate buffer 50 mM, pH 6.5 (H_2O/D_2O, 9/1)	NH_2 (Asp1), His6, His13, His14	3
Ac-Aβ(1-16)	2 mM in phosphate buffer 50 mM, pH 6.5 (H_2O/D_2O, 9/1),	His6, Glu11, His13, His14	4
Aβ(1-28)	0.4 mM, 100 mM SDS, pH 7.5, D_2O, 298 K.	NH_2 (Asp1), His6, Glu11, His13, His14	5
Aβ(1-16) PEG	2 mM pH 7.0, D_2O, 300 K	NH_2 (Asp1), His6, His13, His14	6
Aβ(1-16)	300 μM in TRİS buffer, pH 7.4, D_2O, 318 K.	His6, His13, or His14, Glu11, COO^-	7

Table 2. Different models for Cu:Aβ from experiments.

Fragment/Peptide	**Experimental conditions**	**Proposed binding sites**	**Refs.**
Aβ(1-16)	**50 mM NaPi, 75 mM NaCl, 20 K, pH 7.2**	**Asp1, His6, His13, His14**	8

Aβ(1-40)	**HFIP, 100 mM TRIS, 150 mM NaCl, pH 7.4, 50% glycerol, 310 K**	**N?, N?, N?, O?**	9
Aβ(1-16), Aβ(1-28), Aβ(5-23), Aβ(17-40), Aβ(1-40)	**20 mM Tris-HCl, pH 7.4, 310 K**	**His6, Tyr10, His13, His14, H_2O**	10
Aβ(1-28)	**50 mM N-ethylmorpholine, pH 7.4, 298 K**	**N-terminus, His6, His13, His14**	11
Aβ(1-16), Aβ(1-28)	**pH 4.5 - 8, 298 K**	**N-terminus, Asp?/Glu? His13, His14**	12

Table 3. Calculated conformational enthalpy, solvation Gibbs free energy, entropy and conformational Gibbs free energy for Cu(II):Aβ(1–40) and Cu(II):Aβ(1–42) along with the corresponding values for Zn(II):Aβ(1–40), Zn(II):Aβ(1–42), apo Aβ(1–40) and apo Aβ(1–42).

Metallopeptide	**$\langle G_{sol} \rangle$ (kJ mol^{-1})**	**$\langle H_1 \rangle$ (kJ mol^{-1})**	**$-T\langle S_1 \rangle$ (kJ mol^{-1})**	**$\langle G_{sol} \rangle$ (kJ mol^{-1})**
Cu(II):Aβ(1–40)	−2174.9 (± 30.8)	−1998.8 (± 46.1)	−2109.0 (± 12.8)	−4107.7 (± 33.8)
Zn(II):Aβ(1–40)	−2.235.9 (± 24.9)	−2979.8 (±16.3)	−2.096.2 (± 28.5)	−5076.0 (± 20.6)
Apo Aβ(1–40)	−2007.7 (± 125.9)	−2788.2 (± 55.6)	−2114.4 (± 9.9)	−4902.5 (± 45.9)
Cu(II):Aβ(1–42)	−1911.6 (± 14.4)	−2072.7 (± 19.4)	-2177.6 (± 3.2)	−4250.3 (± 16.6)
Zn(II):Aβ(1–42)	−2183.2 (± 28.8)	−2908.3 (± 12.1)	−2189.1 (±29.3)	−5097.4 (±21.0)
Apo Aβ(1–42)	−2404.5 (± 27.3)	−2579.9 (± 24.2)	−2206.6 (± 4.1)	−4786.5 (± 20.3)

Figures:

Figure 1. The sequence of Aβ42, which can be divided into four regions: the metal-binding region, the central hydrophobic core region, the central polar region, and the C-terminal hydrophobic region. Residues labeled as red, blue, green, and black are negatively charged, positively charged, polar, and hydrophobic, respectively. Reproduced with permission from John Wiley and Sons: Liao *et al.*[133]

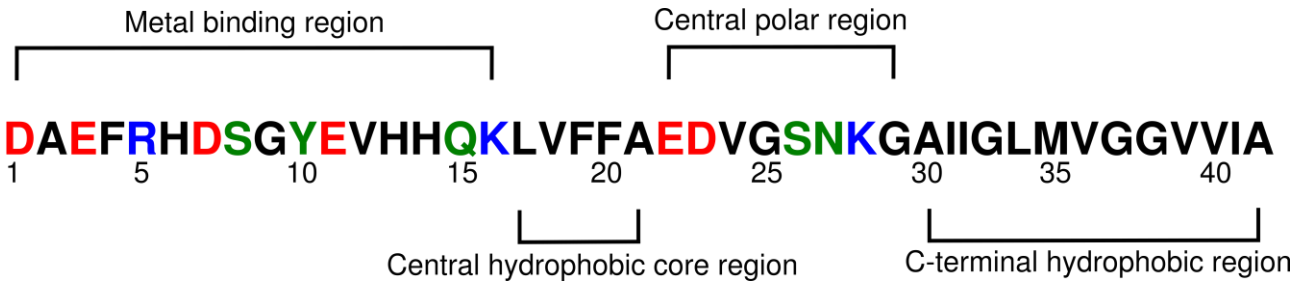

Figure 2. Optimized structures of a) Cu:$(His)_3$Asp, b) Cu:$(His)_3$Glu and c) Cu:$(His)_3$Tyr coordination complexes at the B3LYP/6-31G* level of theory in the gas phase. The atom names are according to the AMBER force field. Reproduced with permission from John Wiley and Sons: Wise and Coskuner.[145]

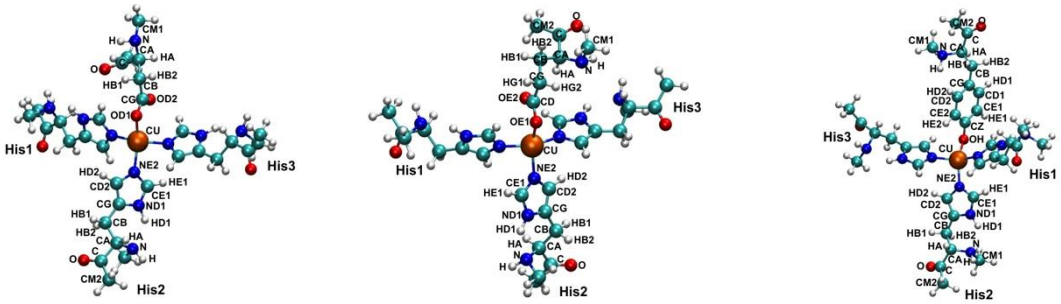

(a) (b) (c)

Figure 3. ONIOM-optimized structures of Fe(II)−heme−Aβ(H13)a and Fe(II)−heme−Aβ(H13)b (inset) showing details of the bonding environment of the heme. The heme group and the side chain of His13 constitute the QM part. ΔG(aq) is relative to Fe(II)−heme−Aβ(H13)a in kJ/mol. Reprinted with permission from S. Azimi and A. Rauk, The Binding of Fe(II)–Heme to the Amyloid Beta Peptide of Alzheimer's Disease: QM/MM Investigations, J. Chem. Theory Comp. 2012, 8(12):5150-5158, Copyright (2018) American Chemical Society.

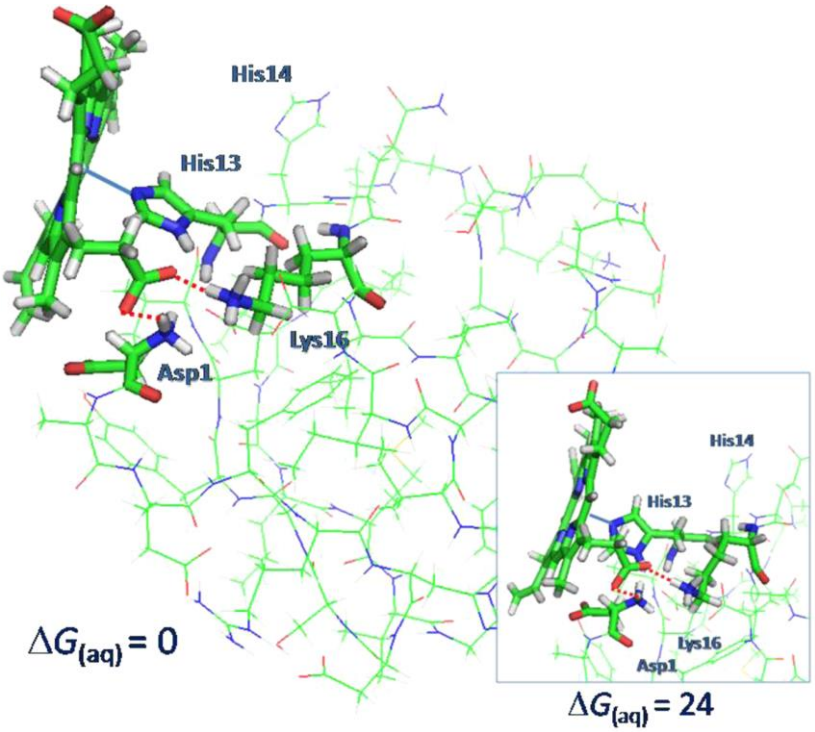

Figure 4. (A) Schematic illustration of the Cu(II) dummy model. Instead of a simple sphere, the point charge of the Cu(II) ion is distributed to six dummy atoms (in grey) with partial charges (shown in blue), leading to a formal charge of –1 (shown in red) at the central atom (in orange). Different charges for the equatorial and axial dummy atoms along with different bond lengths between these and the central atom allow to reproduce the Jahn-Teller effect in classical MD simulations of the Cu(II) ion. (B) Snapshot from a 100 ns MD simulation of the Cu(II) dummy model coordinated to Aβ16 via the carbonyl O atom of Ala2, Nδ of His6, Nε of His13, and Nδ of His14. The ligating residues were allowed to choose their preferred dummy atom to interact with. Two water molecules interacted with the remaining two dummy atoms during the MD simulation. Aβ16 is shown in cartoon with the N- and C-terminus being indicated by a blue and red sphere, respectively. The ligating residues and water are shown in Corey−Pauling−Koltun (CPK) presentation using turquoise for C, blue for N, red for O, and white for H atoms. Reprinted with permission from, Q. Liao, S. C. L. Kamerlin, B. Strodel, Development and Application of a Nonbonded Cu2+ Model That Includes the Jahn–Teller Effect, Phys. Chem. Lett. 2015, 6(13):2657-2662, Copyright (2018) American Chemical Society.

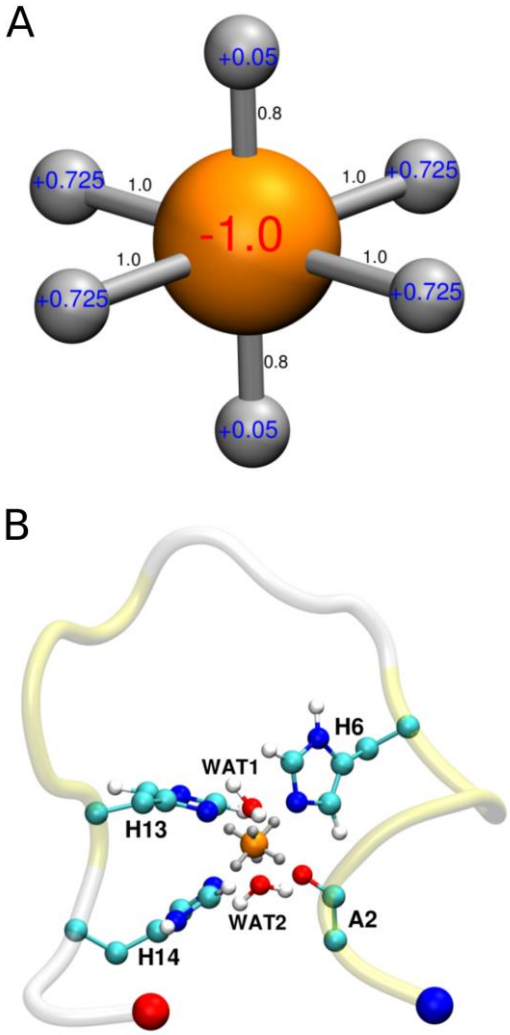

Figure 5. Potential of mean force (ΔPMF) of (a) Zn(II):Aβ40 and (b) Zn(II):Aβ42 structures along the coordinates representing the radius of gyration (R_g) and end-to-end distance ($R_{E\text{-}E}$). Reprinted with permission from O. Wise-Scira, L. Xu, G. Perry, O. Coskuner, Structures and free energy landscapes of aqueous zinc(II)-bound amyloid-β(1–40) and zinc(II)-bound amyloid-β(1–42) with dynamics, J. Biol. Inorg. Chem. 2012, 17(6):927-938, Copyright (2018) Springer Nature.

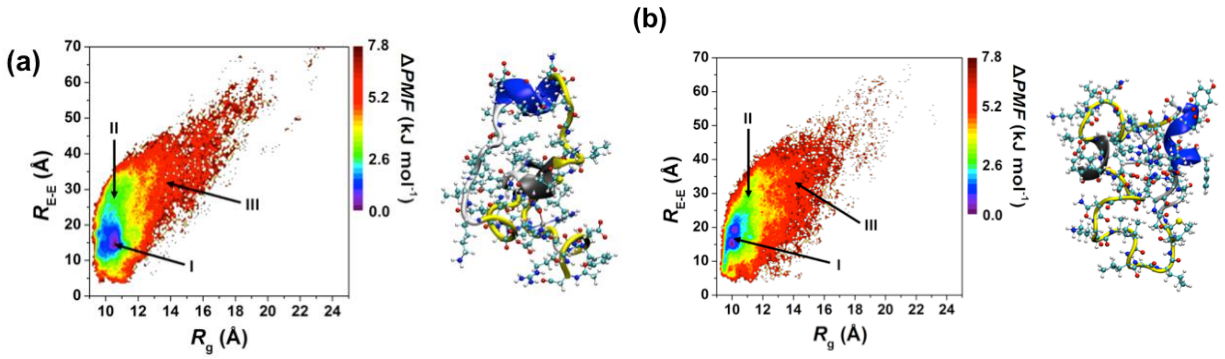

Figure 6. Probabilities of the different secondary structures are shown per residue of Zn:Aβ40 (black) and Zn:Aβ42 (red) in aqueous solution. The π-helix and coil structures are not displayed. Reprinted with permission from O. Wise-Scira, L. Xu, G. Perry, O.

Coskuner, Structures and free energy landscapes of aqueous zinc(II)-bound amyloid-β(1–40) and zinc(II)-bound amyloid-β(1–42) with dynam-ics, J. Biol. Inorg. Chem. 2012, 17(6):927-938, Copyright (2018) Springer Nature.

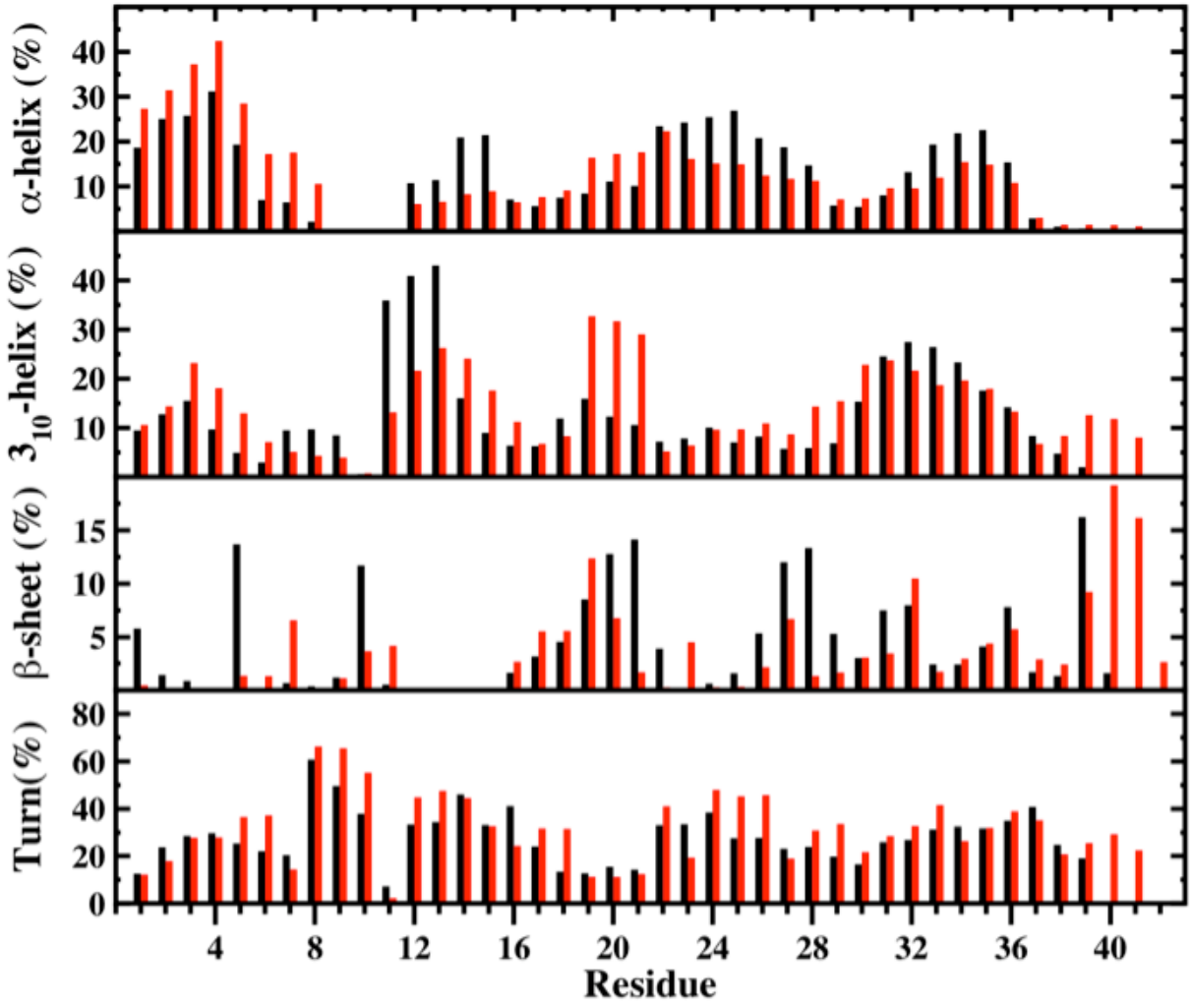

Figure 7. Correlation between the (A) C_α and (B) H_α chemical shift values for metal free Aβ42 at 280 K using the structures from the simulations of Coskuner (δsim.) and experimental (δexp.) chemical shift values provided by Prof. Michael Zagorski.[143] The Pearson correlation coefficients are 0.980 and 0.930 for the C_α and H_α chemical shifts, respectively. Reprinted with permission from O. Wise-Scira, L. Xu, G. Perry, O. Coskuner, Amyloid-β peptide structure in aqueous solution varies with fragment size, J. Chem. Phys. 2011, 135(20):205101, Copyright (2018) American Institute of Physics.

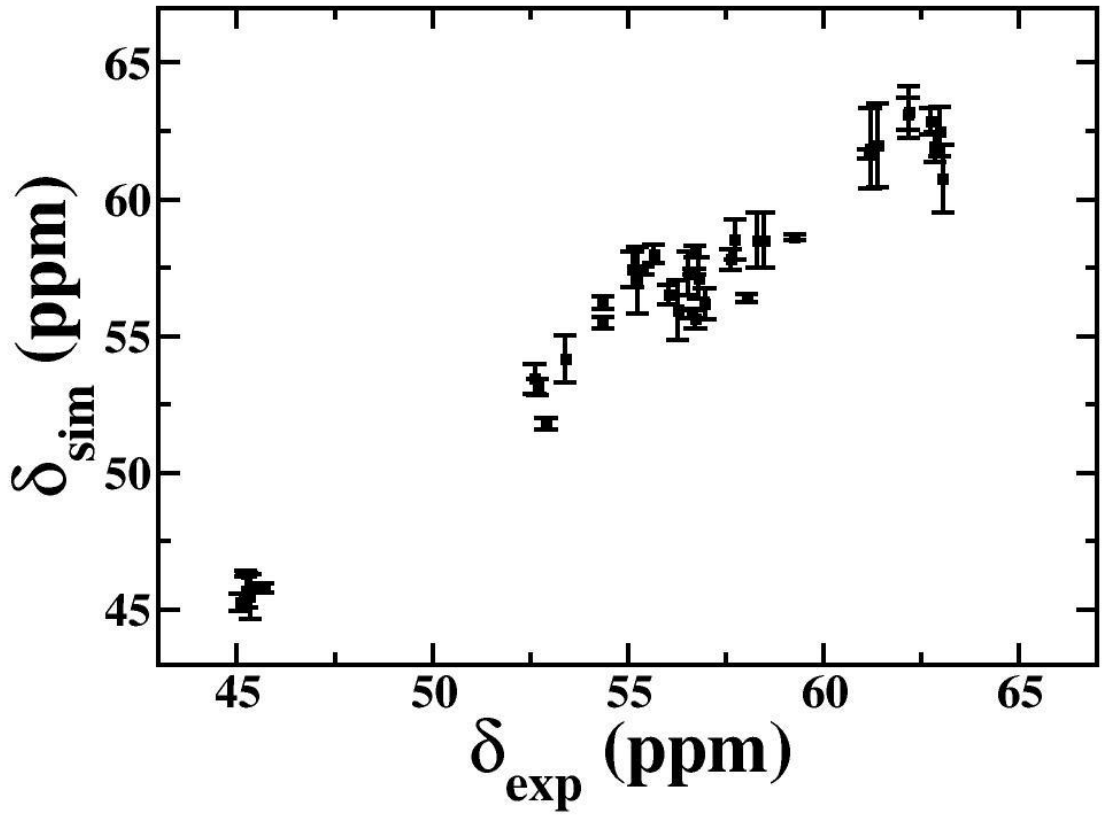

(a)

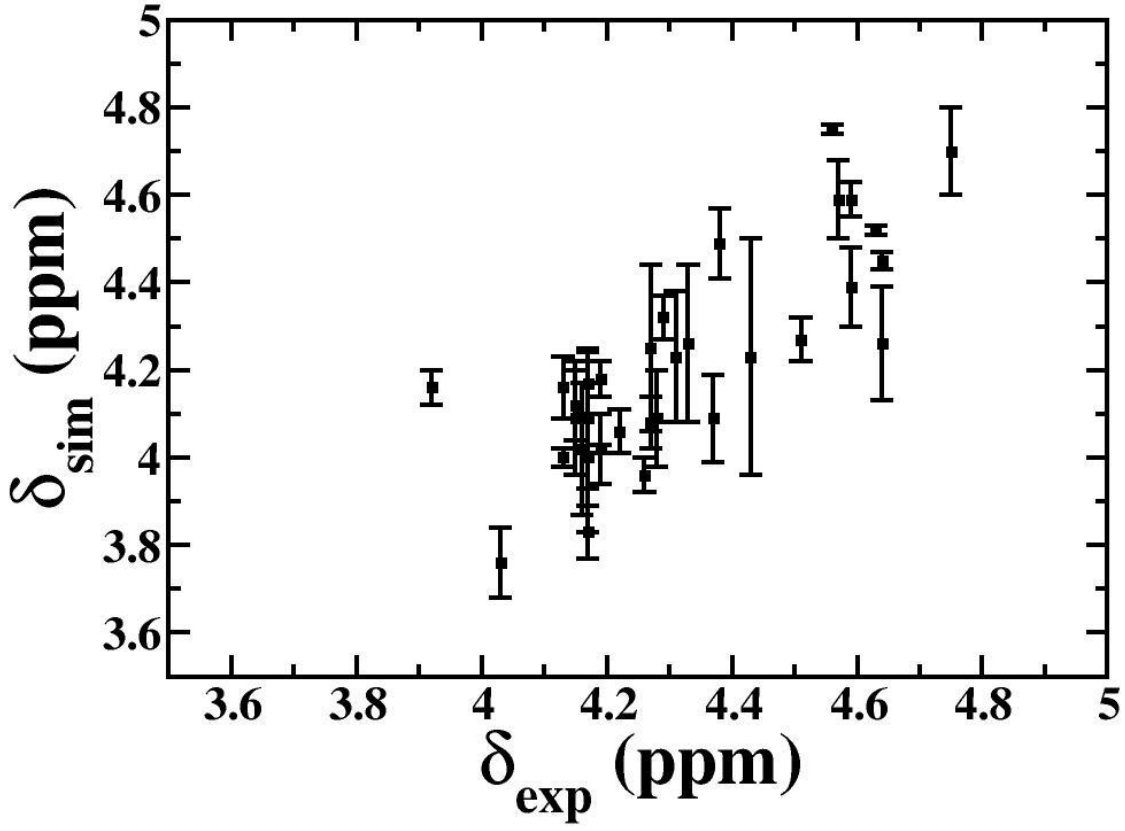

(b)

Figure 8 Secondary structure probabilities per residue of (A) Aβ40 and (B) Aβ42 in aqueous solution. Results are shown for the apo state of both peptides (black) and Cu(II)-bound with the Cu(II):$(His)_3$Asp1 (red), Cu(II):$(His)_3$Glu11 (blue), and Cu(II):$(His)_3$Tyr10 coordination modes. The π-helix and coil structures are not displayed. Reprinted on written permission of JOTCSA editorship (2018).[43]

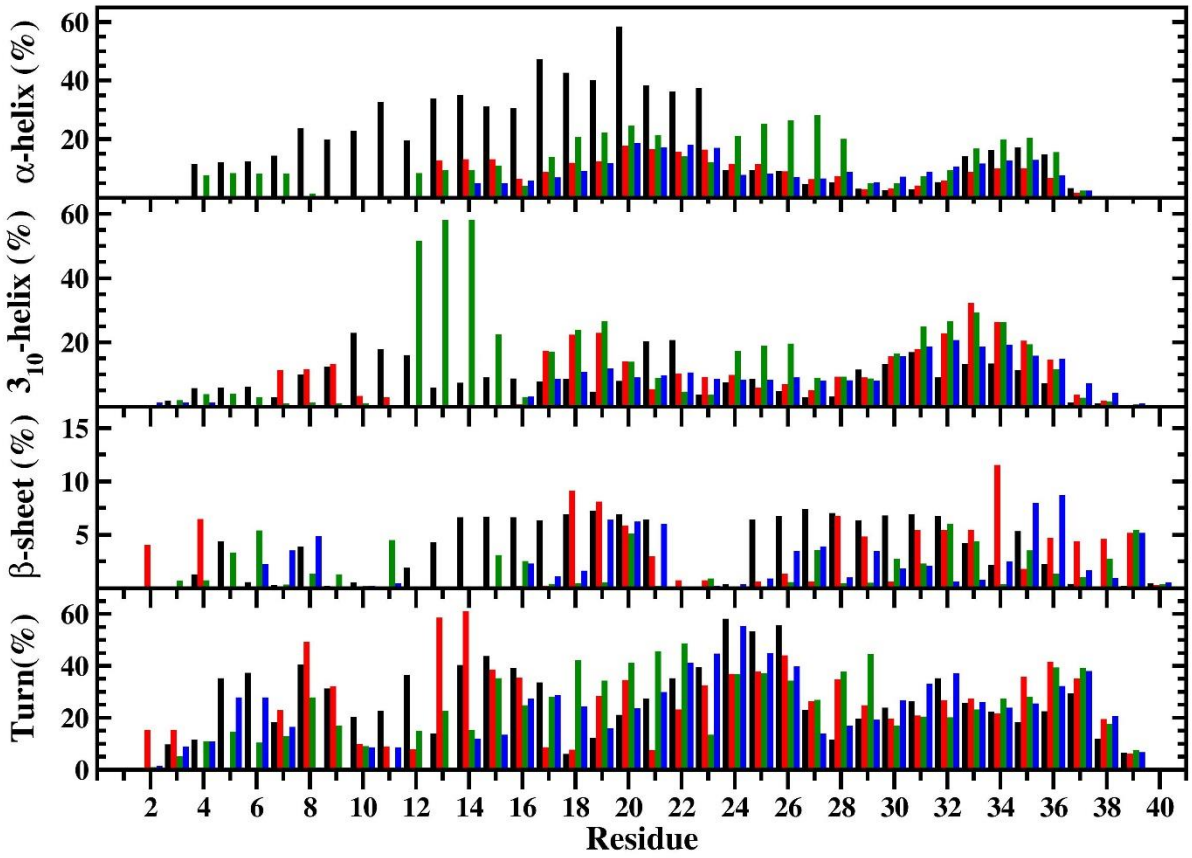

Figure 8B. Residual Secondary Structure Abundances of the apo and Cu(II)-bound Aβ42 Peptides. Secondary structure abundances per residue of the Aβ42 (black), Cu(II):His3Asp1-Aβ42 (red), Cu(II):His3Glu11-Aβ42 (blue), and Cu(II):His3Tyr10-Aβ42 (green) structures in an aqueous solution. The π-helix and coil structures are not displayed. Reprinted on written permission of JOTCSA editorship (2018).[43]

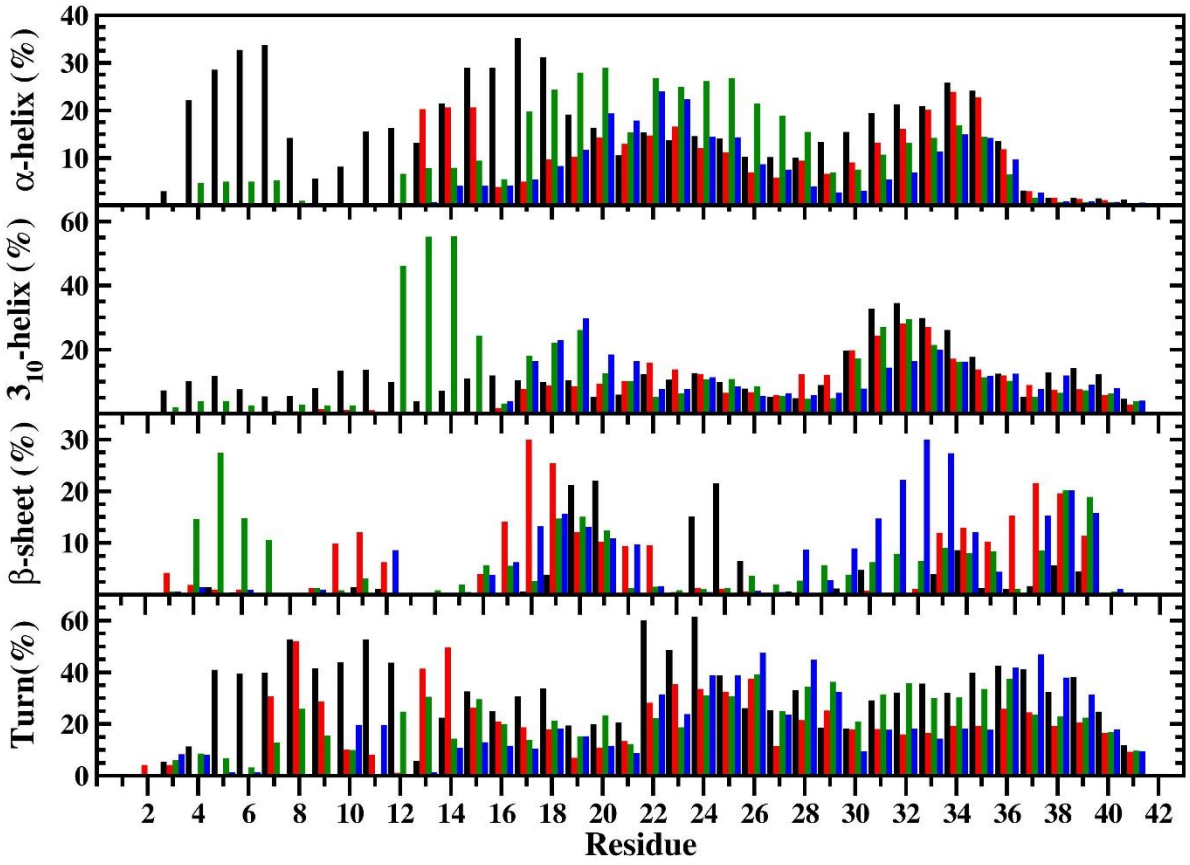

Figure 9. Transition networks for (A) the Aβ42 dimer and (B) the Cu(II)-bridged Aβ42 dimer, where the Cu(II) ion was coordinated by a pair of His13 and His14 residues from the two Aβ42 peptides. The nodes of the transition networks correspond to different dimer states, which are characterized by the numbers of residues in α-helix and β-sheet conformation given as α|β. The area of a node is proportional to the population of the underlying state and the color indicates the structural preference as indicated in the color bar. The thickness of the edges correlates with the transition probability between the two nodes connected by the edge in question. It can be seem that Cu(II) binding induces the formation of β-sheets (more and larger nodes shown in blue), which can be also seen from the representative structure of the highest populated node for (C) the Aβ42 dimer and (D) Cu(II):(Aβ42)2. The peptides are rendered as a cartoon with one peptide of the dimer shown in red and the other one in blue. The N-terminus of each peptide is indicated by a sphere and β-bridges are marked by violet spheres. In the Cu(II):(Aβ42)2 system, Cu(II) is shown as yellow sphere and the His13 and His14 residues bound to it as sticks. For both conformations the number of residues in the α|β conformation is given.

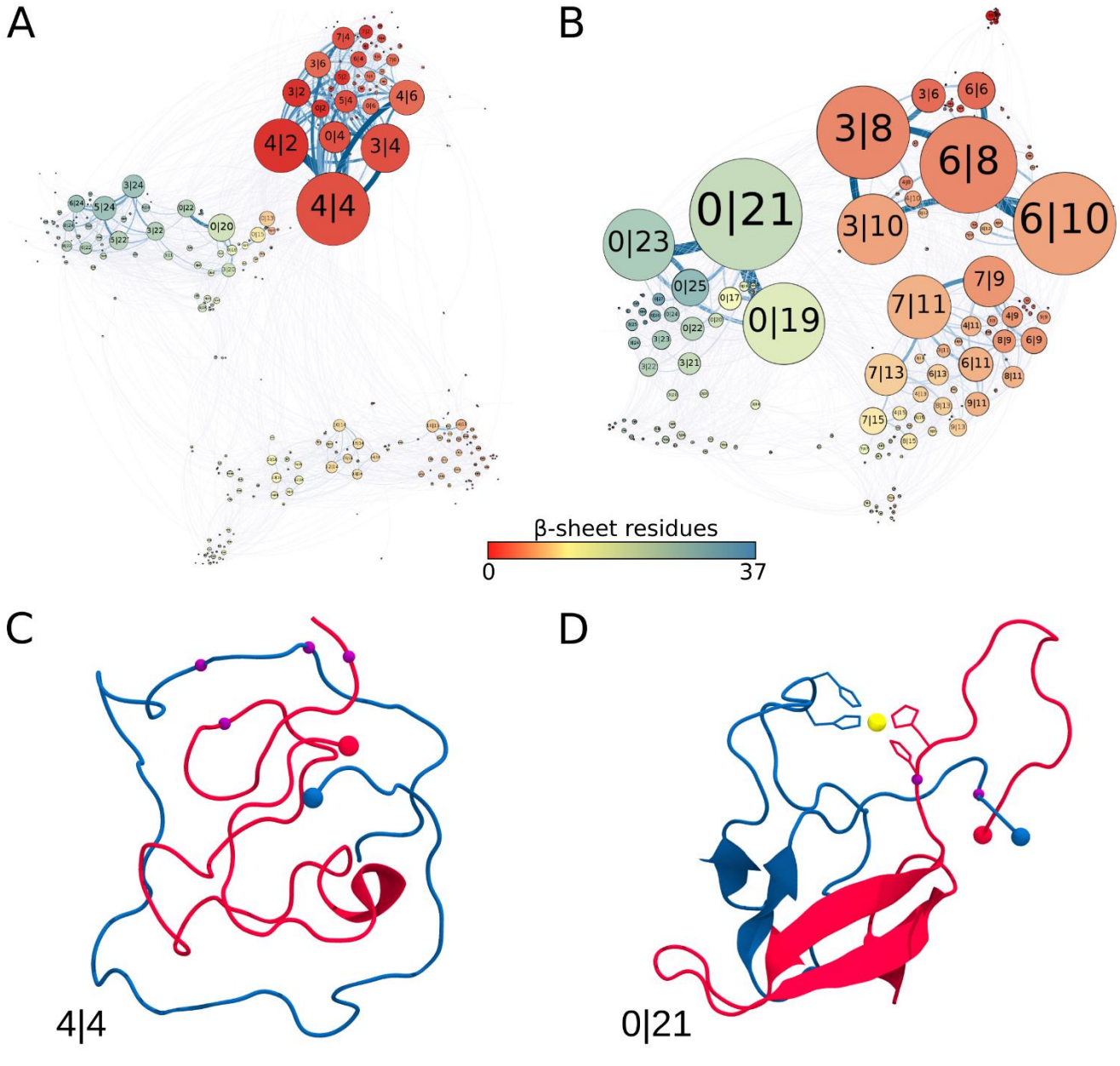
A
B
4|4
4|2
4|6
3|4
0|4
0|20
0|21
0|23
0|19
3|8
6|8
6|10
3|10
7|11
β-sheet residues
0
37
C
4|4
D
0|21

Table of Contents Figure